TÉCNICO LISBOA

Analyses of Solutions for the Attenuation of Cogging Torque in Flux Switching Electrical Generators with Permanent Magnets in the Stator

José Lopes da Silva

Thesis to obtain the Master of Science Degree in

Electrical and Computer Engineering

Supervisor: Prof. Paulo José da Costa Branco

Examination Committee

Chairperson: Prof. Rui Manuel Gameiro de Castro

Supervisor: Prof. Paulo José da Costa Branco

Member of the Committee: Prof. Silviano Francisco Santos Rafael

May 2016

Abstract

The study of Flux Switching Generator with Permanent Magnets in the Stator has gain relevance due to new developments made in permanent magnets, giving this type of machine high power density. However this is correlated with increases torque ripple.

In order to attenuate this torque ripple, this dissertation proposed a flux-switching generator using two coupled rotors, so that the electromagnetic forces applied to each rotor would cancel other out. Using a 3D finite elements modelling analysis, it was possible to study its magnetic flux distribution and electromagnetic forces. Simply by using two-coupled rotors, it was registered a 60% decrease in torque ripple when in a no load functioning, however a consequence of achieving a smaller torque ripple was the reduction of electromotive force. In this context, a series of evaluative magnetic circuit geometries were explored until the final 3D generator was reached, not only significantly reducing the torque ripple but also minimized the electromotive force loss.

To simulate the behaviour of the proposed flux-switching PM generator with an electric load, it was used an AC/AC converter connected to a simplified version of a boing 767 electrical load. The currents generated by this resulted in the appearance of back-EMF, which decreased total EMF output. The armature reaction also influenced the magnetic energy distribution resulting in increased torque ripple for each individual rotor, but decreased the total torque ripple of the model to under 5% when compared with the one in a no-load case.

Keywords: Cogging torque; Electric Machine; Finite elements; Permanent magnets; Switch flux generator.

Resumo

Devido aos desenvolvimentos em ímanes permanentes, o estudo de Máquinas de fluxo comutado com ímanes permanentes no estator tem vindo a ganhar relevância devido a sua elevada densidade de potência. Contudo isso está relacionado com elevados níveis de binário oscilatório.

A solução proposta para a redução do binário oscilatório consiste na utilização de dois rotores acoplados. Estes estarão dispostos de maneira às forças aplicadas num cancelem as forças aplicadas no outro. Para tal, foi feita uma análise em elementos finitos que permitiu obter o comportamento do fluxo e da energia magnética. No caso de não existirem correntes nas bobines, a utilização dos dois rotores resultou numa redução de 60% do binário oscilatório. Contudo a uma consequência da redução do binário oscilatório foi a perda de força electromotriz. O modelo obtido, baseado numa geometria 3D, resultou num redução significativa do binário oscilatório minimizando ao mesmo tempo as perdas de força electromotriz.

O efeito da carga no modelo foi simulado usando um conversor AC/AC ligado a uma versão simplificada dos componentes eléctricos de um boeing 767. O ligar da carga resultou no aparecimentos de correntes nas bobines que gerou uma força electromotriz inversa, esta reduz o valor da força electromotriz de saída. Mais significativo, foi o efeito que as correntes tiveram na energia magnética. Apesar de individualmente, o binário oscilatório de cada rotor ter aumentado, ao combinar o contributo dos dois, reduz para menos de 5% do seu valor sem carga, tornando-o insignificante.

Palavra chave: Binário oscilatório; Elementos Finitos; Gerador de fluxo variavel; Magnetos permanents; Maquinas Electricas.

List of symbols

ϕ	Induced magnetic flux [Wb]
B	Magnetic field [T]
S	Area that the magnetic flux crosses $[m^2]$
H	Induced magnetic field $[Wb/m^2]$
h	Heat transfer coefficient $[W/(m^2 * K)]$
J	Current density $[A/m^2]$
g	Air-gap length [m]
l_m	Permanent magnet length [m]
N	Number of turns in the winding
i	Current in the winding [A]
B_R	Remanent magnetic field [T]
R	Magnetic reluctance $[H^{-1}]$
μ_m	Relative magnetic permeability of the permanent magnet $[Hm^{-1}]$
μ_0	Magnetic permeance of the vacuum $[Hm^{-1}]$
Y	Magnetic permeance [H]
U	Voltage in the winding [V]
T_{el}	Electromagnetic torque [Nm]
T_{ri}	Torque ripple[Nm]
W_m^c	Magnetic co-energy [Ws]

List of abbreviations

AC	Alternate current
AWG	America Wire Gauge
DC	Direct current
DSPM	Double salience permanent magnets
EM	Electric machine
EMF	Electromotive force
FEM	Finite element model
FFT	Fast Fourier Transform
FSM	Flux-Switching Machine
FSPM	Flux-switch Permanent Magnet
IST	Instítuto Superior Técnico
LC	Inductor-capacitor
NdFeB	Neodymium Iron Boron
1ø	One-phase
PM	Permanent Magnet
PWM	Pulse-Width Modulation
R	Resistance
RFPM	Reversible flux permanent magnets
RMS	Root mean square
RL	Resistor-inductor
3ø	Three-phase

List of figures

List of tables

Acknowledgments

Firstly, I would like to thank Professor Paulo Branco for the support and patience. Without his help this dissertation would never have come to life. Secondly, to my colleagues, the discussion we had were fundamental in developing this work and your company was vital to make me push onward.

To my friends, thank you for all the years you have given me, the nights out and the joy you bring to my life. A big thanks to my family for allowing me to reach this far. The support, the opportunities, the care and the love you have given me always gave me the tools to move forwards in life with no regrets. To my girlfriend, for all the life and joy you have brought to my day to day routines, living wouldn't be the same without you.

Since I enrolled in this university, my parents always told me "It was always the dream of your grandmother to have a grandson graduating from IST". Her wish was only made possible with the help of my family, friends, teacher and colleagues, thank you for everything.

Contents

1 Introduction

1.1 Motivation and Defining the Problem

Electric machines with permanent magnets in the rotor have gain the spotlight of the industry due to their high performance. The presence of permanent magnets (PM) in the rotor of electric generators can cause significant setbacks. Being the most common ones the increased air-gap due to the need of mechanical attachments and the possibility of demagnetization. Depending on the application of the generator, there may be significant mechanical stresses on the PM, due to centrifugal forces, which may alter its magnetic characteristic and consequently compromise the structural integrity of the machine.

These problems are mainly caused by the mechanical stress the PM are subdued too. Nowadays, gears can be used to reduce the rotation speed of the PM, however, in doing so, the electromagnetic force (EMF) is limited and power losses increase.

In order to solve those PM structural vulnerabilities it will be studied the possibility of placing them in the fixed part of the electric machine (EM). This change allows a “safer environment” for the magnets, but even though this new design removes centripetal force, reducing the probability of PM’s demagnetizing, the issue of significant torque ripple in this type of electric machines still remains.

The torque ripple is responsible for vibration in the machine, gradually deteriorating it. In a low-speed generator, this torque effect will not be a major concern, in principle. However, when rotating at very high speeds, for example when, coupled in a plane turbine, a small torque ripple could increment with the speed increase, thus resulting in drastic effects.

Recently, an IST master thesis has studied a solution generally called flux-switching machine (FSM) in which the PMs were located in the stator, instead of in the rotor, to increase the mechanical strength of the generator and mitigate possible demagnetizing effects. However, the results obtained in the master thesis held by student Ricardo Mauricio [2] clearly indicated that this electric machines features two main drawbacks: significant iron power losses; and significant torque ripple.

Taking into consideration the previous context, this dissertation studies possible magnetic circuit solutions at a 2D or 3D magnetic circuit modelling level, particularly their electromechanical characteristic in terms of torque ripple reduction and the viability of the generator.

1.2 Theme framework in electrical and computing engineering

The theme of this master dissertation falls within electrical and computing engineering in the field of Applied Electromagnetism and Energy Conversion. The dissertation is relevant duo to the need of maximizing the performance of electrical machines and minimizing vibrations.

The development of a FSM with no torque ripple can be separated into two stages: firstly finding the “best” magnetic circuit geometry for the machine that will contradict the leftover torque ripple to minimize its amplitude, secondly commanding the generator’s electric currents to minimize the torque ripple.

Analysing the various proposed models for switch flux machines will require an understanding of the behaviour of the magnetic flux when altering the magnetic reluctance. The study of the flux and the forces resulting from the interaction between the rotor and the stator will interfere with the resulting torque of the machine. This additional torque result in vibration.

For a better usage and longer life span of the material, these vibrations should be filtered out. If not, in time, this may cause the rotor to get out of alignment which would induce higher oscillation, ultimately, it could result in having parts of the machine destroyed.

The concept is to have the forces applied by the stators on the rotor to counteract each other. Even though they might have different amplitudes, the sum of them could result in a decrease of the value of the ripple. Furthermore, the use of a 3D path, for the magnetic flux, may increase the power density of the machine.

Another way of preventing torque ripple will be studied, through the manipulation of manipulating the current density in the windings. By conducting a harmonic analysis of the torque, one can obtain the necessary current that may nullify the oscillations in its whole.

The aim of this work is to try to obtain a design that nullifies torque ripple. This being said, aiming towards a machine with no torque or speed oscillation at any given speed. All significant models will be subdued to a finite elements study, so that in every case, magnetic dispersion is included in the study and later on.

1.3 State of the art

With World War 2 and the race for armoury, missile development was a priority, with it, a considerable increase in the electric power this weapons required. Instigating the development of flux switching permanent magnet generators in the late 1940s. By the late 1950s its use on large or small weaponry was already common.

In 1955, Raunch and Johnson, proposed for the first time, a topology where the magnets are placed in the stator and a solid single piece rotor. However due to limitations in the permanent magnets of the time, this design was put aside. The robust structure this topology offers, allied with the new developments in permanent magnets, allowed this type of machines to regain the spotlight with ease.

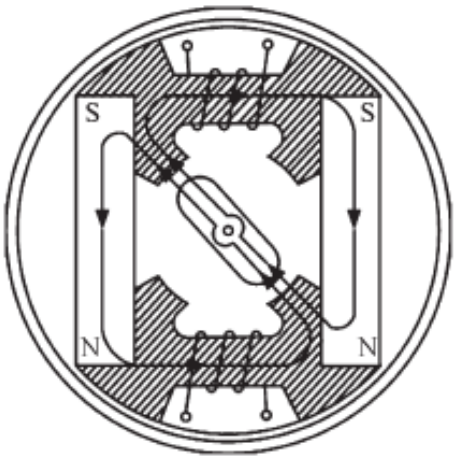

Figure 1-Simple flux-switching alternator, Rauch and Johnson's proposed topology.

There are 3 main types of magnetic reluctance electric machines: double salience permanent magnets (DSPM), reversible flux permanent magnets (RFPM), flux switching permanent magnets (FSPM). Due to the way the magnetic flux travels and the placement of the electric circuits these machines are considered radial.

DSPM machine are the ones that better resemble the common switch flux alternator. The permanent magnets are placed in the inner part of the stator. The flux however is not reversible, Figure 2 (a). RFPM, as the name suggests allow the flux be reversible. The magnets are placed in the stator saliences near the windings. In this case the air gap increases with the magnets length, Figure 2 (b). The FSPM machines are typically more complex. Each permanent magnet as a ferromagnetic material on each side and the windings pass in a hole within that ferromagnetic material. The flux is reversible and its operating principle resembles the initial topology proposed by Rauch and Johnson, Figure 2 (c).

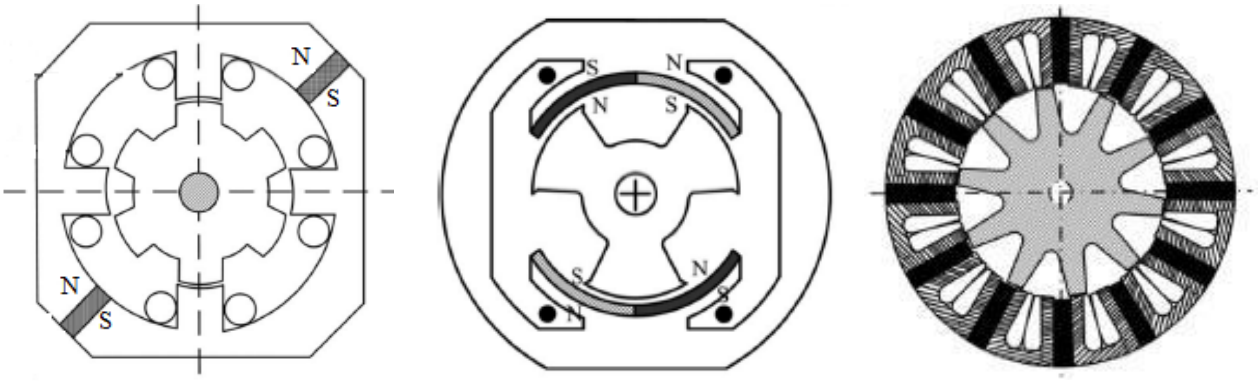

(a) (b) (c)

Figure 2-Permanent magnets machine topology for: (a) DSPM; (b) RSPM; (c) FSPM.

All have one thing in common, they can all be studied using a 2D perspective and all this machines are characterised by a strong torque ripple. All the development being made to counteract this is either changing the rotor teeth shape or injected current control to smooth the transition in the critical areas.

When it comes to changing the rotor teeth shape, the studies in [3] and [4] serve as examples on methods already being studied in order to reduce torque ripple. The results reached in them, although presenting a notable improvement, still presented significant levels of torque ripple.

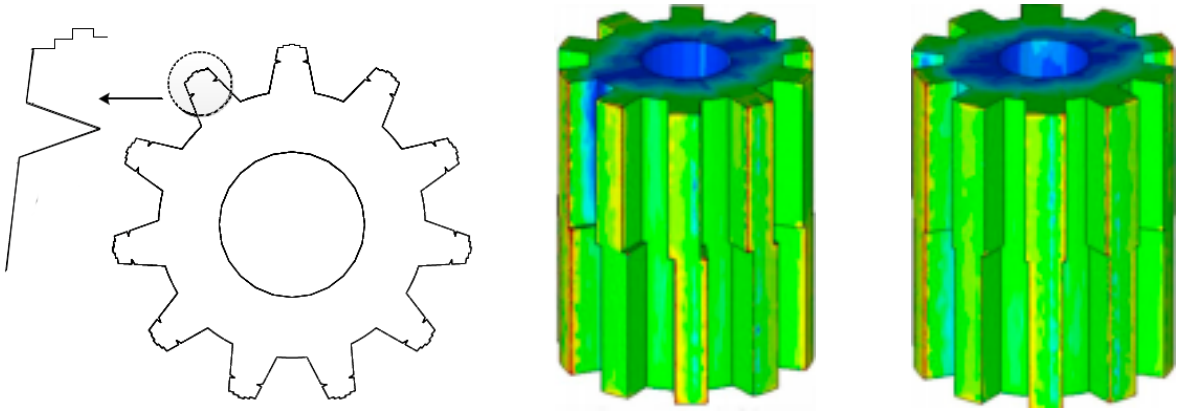

(a) (b) (c)

Figure 3- Rotor configurations studied for torque ripple reduction: (a) proposed in [3]; (b) proposed in [4]; (c) proposed in [4].

As for the injected current control, the studies [5] and [6], showed promising results, with significant reduction of the torque ripple. Manipulation the current harmonic component, by injecting additional higher frequency components resulted in considerable reduced values of torque ripple, however its use requires complex electronics to function. What if the magnetic flux travelled in all axis? Unlike other methods, this study will be focused on, reducing the torque ripple, by having the forces, created by the different rotor saliences, counteract each other and minimizing the magnetic energy variation.

1.4 Documents schematic

The following master dissertation consists in 6 parts. Being the first where the problem is defined explain why it's going to be addressed.

The second chapter consists on an evolutionary process explaining the though behind the changes, and the resulting improvements due to this changes. This evaluation were based on a magnetic circuit approach, studying the magnetic circuit for each model. However, for the 2D model, a FEM analysis was conducted, allowing us to have a better understanding of the forces at hand.

The third chapter, and once the bases model for the machine had be establish, a FEM study was preformed and the results were significantly underperforming. Basing now on FEM analysis, the model suffered a new evolutionary process, resulting in the final design.

Since it was necessary to study the effects of a load on the machine, in chapter four, illustrates the chosen AC/AC converter and load chosen, and the effect this load has on the generator. The effects studied were alterations to: EMF, torque and power losses, due to the currents effect on the magnetic circuit and windings, hysteresis losses and eddy currents.

The fifth and final chapter compiles the final results, contains the conclusions reached in this dissertation and state strengths, weakness, improvements and future work to be made before creating a functional prototype.

2 Evolution of the concept for the final model

2.1 Geometric configuration of a 2D magnetic circuit able to minimize torque ripple: 2D EMF study of the resultant machine

Torque ripple in the rotor may damage the integrity of the electrical machine. Therefore, it is important to minimize torque oscillations. In order to have the rotor's torque ripple diminished, the configuration required for the rotor piece, considering a two-salience stator, is illustrated in Figure 4. The filed excitation circuit is located in the fixed stator, while the rotor moves with an angular speed w as indicated. The rotor is formed by three symmetric displaced saliencies, having their arc length θ_0 equal to the stator arc length θ_1:

$$\theta_0 = \theta_1 \tag{1}$$

Due to the need for stability, the rotor, without external influence, will be pushed to a condition where magnetic reluctance is minimal; this force is represented by a letter F. When a rotor pole is getting aligned with the superior stator's salience, a reluctance force F pulling the rotor appears. When it is getting out of the alignment with the inferior stator's pole, this force will push the rotor back.

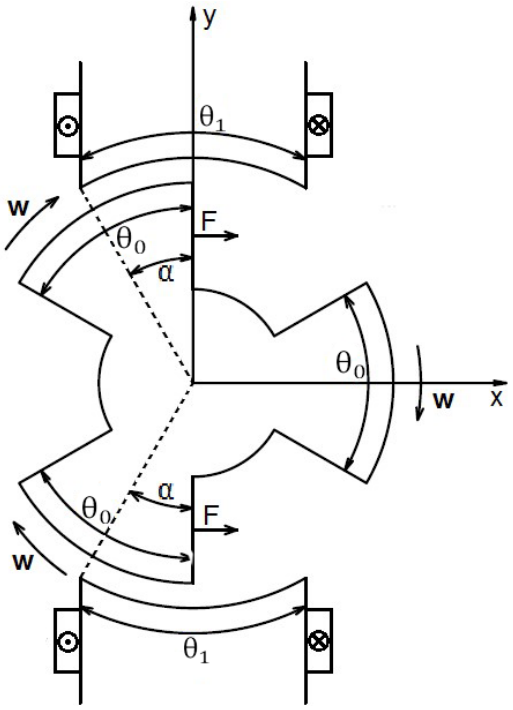

Figure 4-Basic two-salience stator geometric structure to nullify the torque ripple

Figure 5 (a) and (b) shows that when the rotor and stator have different arc length, there will be a “dead-zone” in the electromagnetic torque. Therefore to combat that issue, the rotor pole will need to be as wide as the stator’s pole. Since the rotor, on this example, can be divided into six equal arcs, the angle of each will be given by expression (2):

$$\theta_0 = \theta_1 = 60^o \quad (2)$$

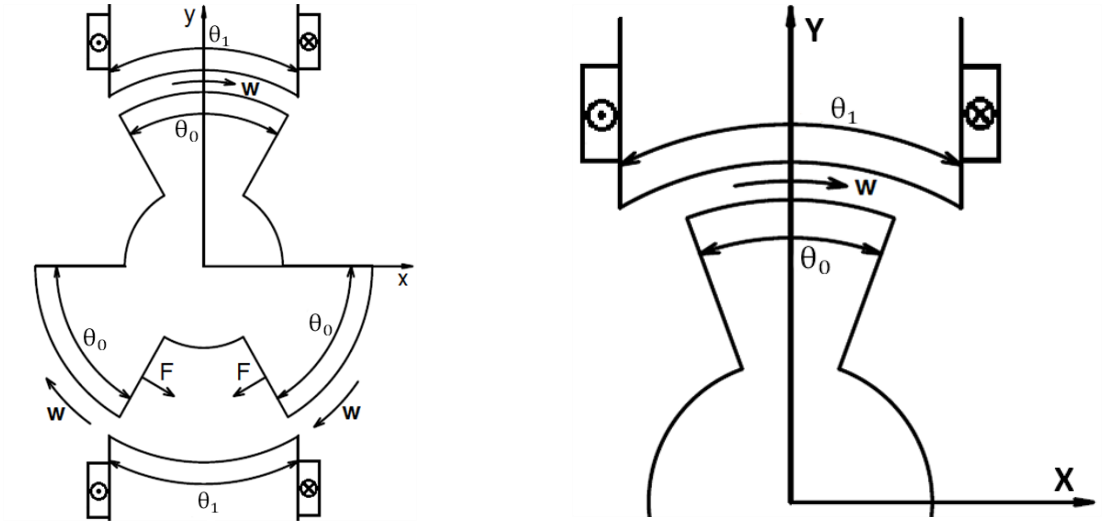

(a) (b)

Figure 5- (a) Rotor and stator poles having the same arc length, (b) Rotor and stator poles with different arc length

In Figures 1 to 3, F is representative of the force applied to the rotor on its quest to find equilibrium. Both in Figure 4 and Figure 5(a) the sum of all forces is null, having no effect on the torque. However in Figure 6, F_a F_b, represent, respectively, the resulting forces from the interaction with the top and bottom stator poles. The smaller the α, from Figure 4, the bigger the force trying to make it larger. This difference in applied forces will be the main responsible for the torque ripple.

During the study of the magnetic circuit no magnetic leakage was taken into account, the core was a ferromagnetic material with high magnetic permeance, the distribution of the magnetic flux along each section was uniform and the rotor’s and stator’s salience were of equal cross section.

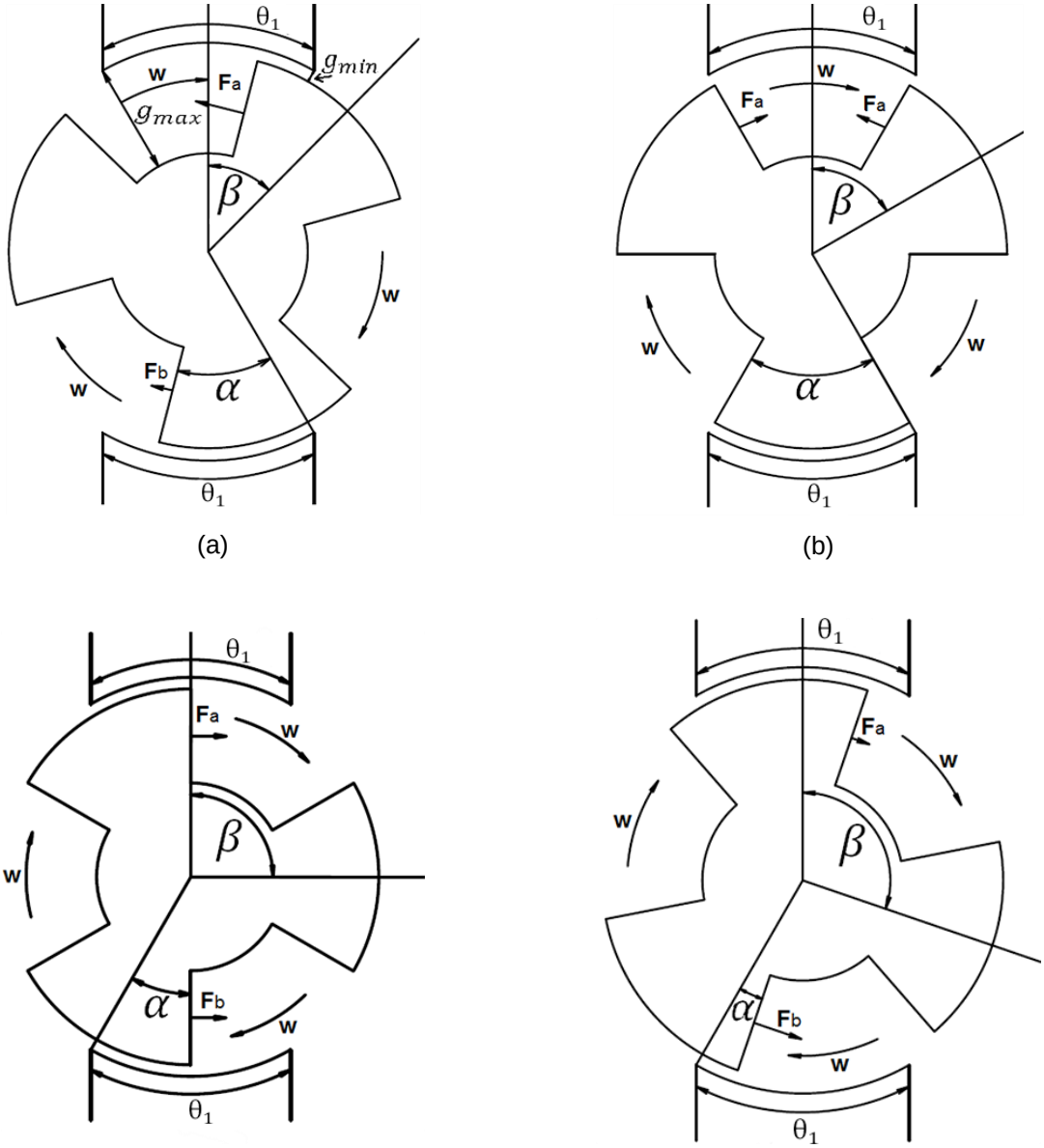

Figure 6 - Forces applied to the rotor at β: (a) 46º; (b) 60º; (c) 90º; (d) 100º

The geometry of the rotor allows the flux to react equally independent of which rotor's pole is facing the stator. Meaning, from the stators perspective, for every full turn of the rotor, it will seem as if the magnetic field, which is only dependent on the magnetic reluctance, varieties thrice. The total magnetic reluctance is only dependent on the angle α between the rotor and the stator saliences, as given by (3). The only variable, of the magnetic reluctance, $\mathrm{R_{air}}$, dependent on α is the salience section exposed to the stator, from a given distance g.

$$\mathrm{R_{air}}(\alpha) = \frac{\mathrm{g}}{\mu_0 \mathrm{S}(\alpha)} \tag{3}$$

$$Y_{airmax}(\alpha) = \frac{\mu_0 S(\alpha)}{g_{min}} \tag{4}$$

$$Y_{airmin}(\alpha) = \frac{\mu_0 S(\alpha)}{g_{max}} \tag{5}$$

By simply using definition (3) the magnetic reluctance would shoot up to infinite values. Such approximation is unrealistic, therefore for better understating on the real evolution of the magnetic reluctance between the rotor and the stator, R_{air} will be studied via its magnetic permeance, Y_{air}. As defined by (6) the permeance will be the weighted sum of the permeance between: the stator and a rotor's pole (4); the stator and the inner part of the rotor (5).

$$Y_{air}(\beta) = Y_{airmax} p(\beta) + Y_{airmin}\big(1 - p(\beta)\big) \tag{6}$$

The weight each part will account for the permeance is given by a percentage p which is directly related to β. As mention before, for every turn of the rotor, the stator will feel as if magnetic field has shifted three times, and (7) will only be valuable the first period, ultimately:

$$p(\beta) = \left|1 - \frac{3}{\pi}\beta\right| ; \beta \in \left[0, \frac{2\pi}{3}\right] \tag{7}$$

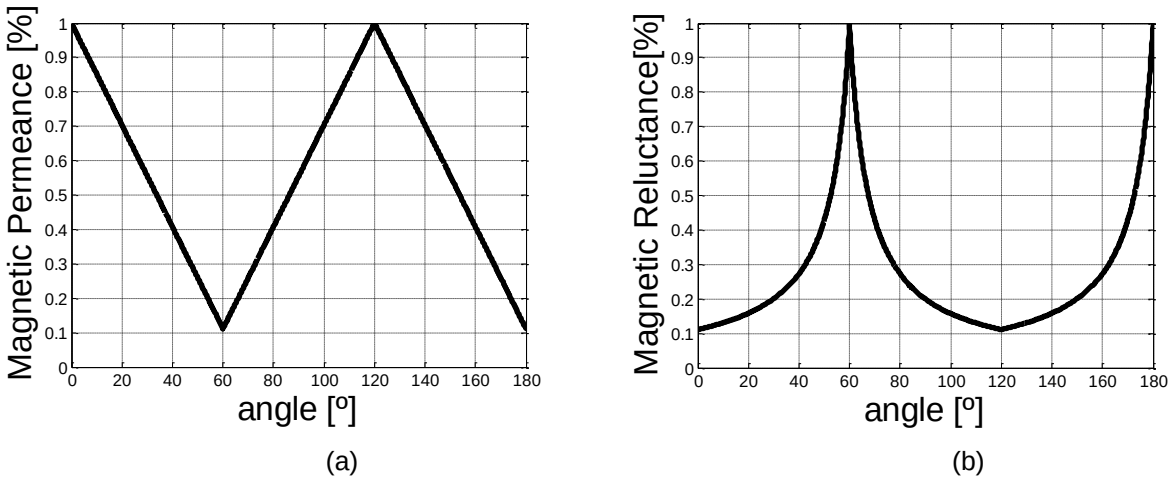

(a) (b)

Figure 7- (a) Magnetic Permeance in a turn, between any pole of the top stator and the rotor; (b) Magnetic Reluctance in a turn, between any pole of the top stator and the rotor

Figure 7 (a) and (b) illustrate how the magnetic reluctance and permeance evolve, in time, for the top half. The reluctance, for example, varies about 6 times from its minimum to its maximum value, indicating the possibility of significant electromotive forces. To note that for the bottom half, the behaviour of the magnetic reluctance is the same with a deviation of 60 degrees. The maximum values for Magnetic permeance and reluctance are respectfully: $4.21 * 10^{-7}[S]$; $2.14 * 10^{7}[\Omega]$.

2.2 Two Independent Stator and One Common Rotor electrical machine analysis

The premise for this machine is that by combining the torques ripple of two separate machines, the stress in the machine's materials would be minimized since cogging torque would be null. On that assumption, the machine would be composed by two independent stators and on common rotor. The two stators would have a rotation of 60 mechanical degrees between each other. This is assumed to have the same effect as mention in [4], for the "Rotor Step Skewed" study.

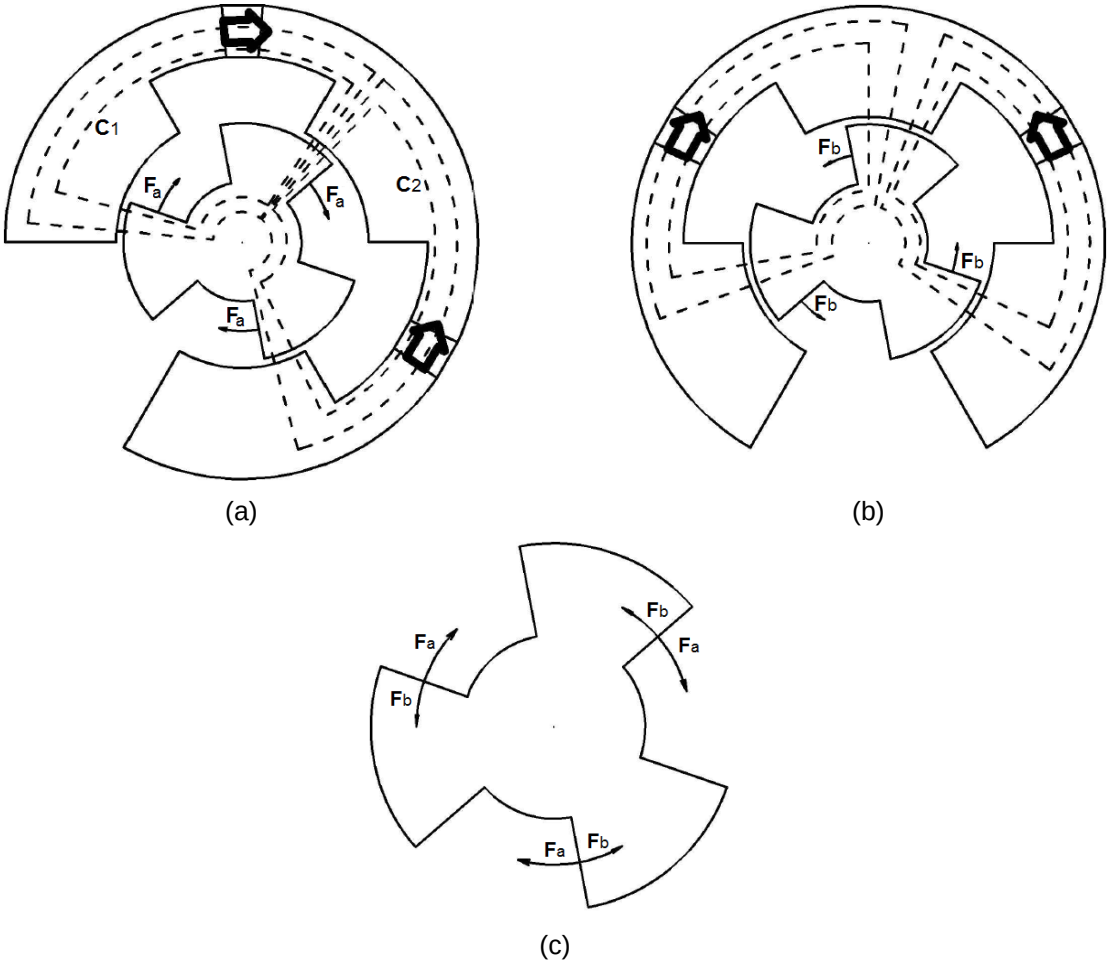

Figure 8- Two stator common rotor geometry: (a) top stator with rotor; (b) bottom stator with rotor; (c) rotor and forces applied by both stators.

Figure 8 (a) (b) and (c) show the two stator parts and the rotor. Each stator has two PMs (Figure 8 (a) and (b)) with opposing magnetizations. As it can be seen, there is an opening in the stators, this is because, with only two magnets, if that segments was closed with iron, there would be no flux passing through it, meaning it wouldn't impact the magnetic circuit.

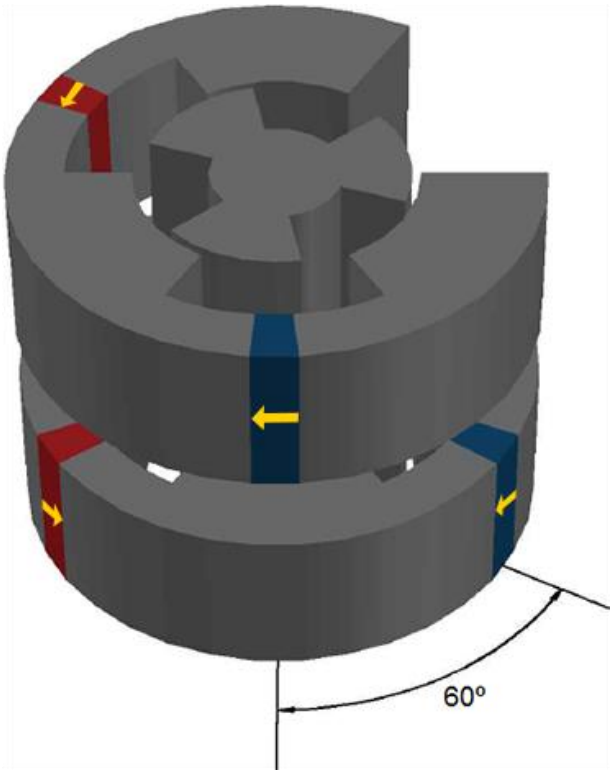

Figure 9- Two stator common rotor geometry

By observing the 3D illustration of the proposed machine, Figure 9, the two stators with a 60 degree rotation the forces applied to the rotor may counter each other, as explicit in Figure 8 (c).

2.2.1 Analyses of the 2D magnetic circuit

To make the analysis of the magnetic circuit, of Figure 10, more tractable but still accurate it is conventional to make the following assumptions:

1. The permeance of the magnetic material is high enough to be assumed infinite;
2. The air-gap length g is assumed small when compared with its transverse dimensions $g << L$, $g << h_1$, $g << h_2$, so that the fringing at the gap edges can be ignored.
3. Leakage flux is assumed negligible.

The specification if infinitely permeable magnetic material implies that $\vec{B} = \mu\vec{H}$ with $\mu \to \infty$. Therefore with a finite $\vec{B}$, the magnetic field $\vec{H}$ is zero inside the magnetic material, occurring only in the air gaps where $\vec{B} = \mu_0\vec{H}$ and in the magnets.

The path of the flux can be represented by C_1 and C_2 in Figure 10 and as it can be observed they mirror each other, meaning they both have the same cross section: S_1, S_2. This will result in equal magnetic

flux, ϕ, passing through windings 1 and 2; however in winding 3 the resulting flux will double, since it's the sum of the two, while having a cross section of equal size. The magnetic flux conservation and the geometry of Figure 10 will results in equation (8).

$$\phi_1 + \phi_2 + \phi_3 = B_3S_3 + B_2S_2 + B_1S_1 = 0 \tag{8}$$

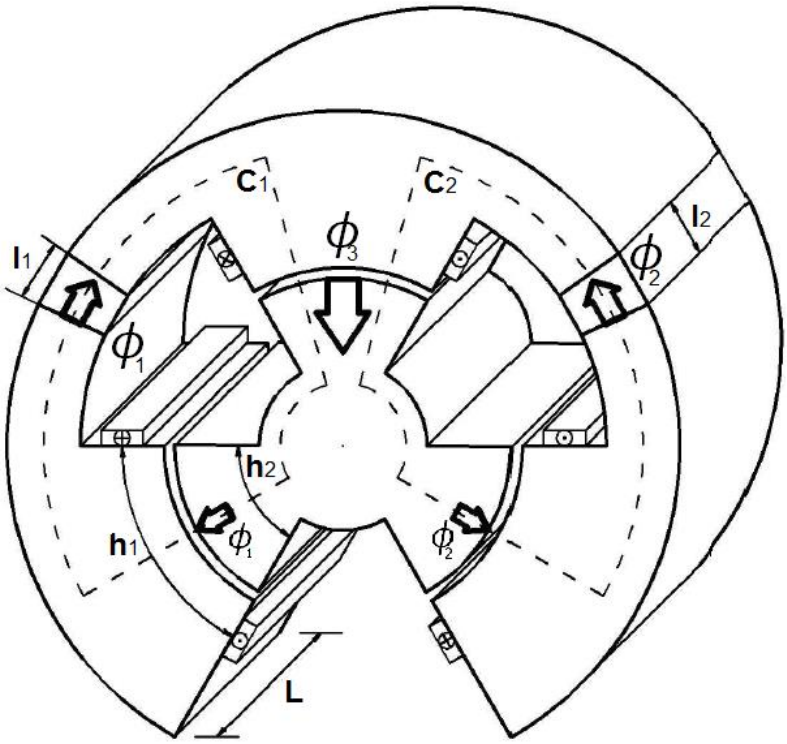

Figure 10- proposed geometry for one half of the electric machine

The use of Ampere's law (9) around contours C_1 and C_2, in Figure 9, result in (10) and (11). On it, one considers the air-gap length, g, the length of the magnets 1 ,on the left, and 2 on the right, as l_1 and l_2 respectfully. The number of turns in each winding, N, and the current in each winding, i_1, i_2 and i_3.

$$\oint_C \vec{H}.\vec{dl} = \int_S (\vec{J}.\vec{n})\, ds \tag{9}$$

In this design the air gap reluctance of any pole of a stator is equal, must be noted that the stator

$$H_{air}2g + H_{m1}l_1 = N(i_1 + i_3) \tag{10}$$

$$H_{air}2g + H_{m2}l_2 = N(i_2 + i_3) \tag{11}$$

With the intensity of the magnetic field in each magnet, H_{m1} and H_{m2}, remanence flux density B_r and their magnetic permeance, μ_m, a linear approximation can be made , resulting in the characteristic of the PM, as shown in equations (12) and (13).

$$B_{m1} = \mu_m H_{m1} + B_r \tag{12}$$

$$B_{m2} = \mu_m H_{m2} + B_r \tag{13}$$

Combining equations (10) and (12), yields equation (14). In there, the magnetic reluctance of each air-gap appears as the only variable, other than the magnetic flux, that is dependent of the mechanical angle, θ, between the rotor and stator. Notice that it has been assumed both magnets to be identical, either their geometry as well as their magnetic characteristic.

$$\begin{bmatrix} 2R_{air}(\theta) + \frac{l_m}{\mu_m S_m} & R_{air}(\theta) \\ R_{air}(\theta) & 2R_{air}(\theta) + \frac{l_m}{\mu_m S_m} \end{bmatrix} \begin{bmatrix} \phi_1 \\ \phi_2 \end{bmatrix} = \begin{bmatrix} \frac{B_r l_m}{\mu_m} + N(i_1 + i_3) \\ \frac{B_r l_m}{\mu_m} + N(i_2 + i_3) \end{bmatrix} \tag{14}$$

The air magnetic reluctance will vary with θ between a minimum and maximum values and, for a simpler perspective, the magnetic permeance, Y_{air}, will be used, which is related with the maximum and minimum reluctances and function of θ as expressed by the two relations in (15) and (16).

$$R_{air,min} = \frac{g_{min}}{\mu_0 S} \tag{15}$$

$$R_{air,max} = \frac{g_{max}}{\mu_0 S} \tag{16}$$

The magnetic permeance of the air-gap is defined by (17) and (18), and the resulting magnetic permeance can be observed in the Figure 7 (a).

$$\text{If } \theta \epsilon \left[0, \frac{\pi}{3}\right] \Rightarrow Y_{air}(\theta) = \frac{1}{R_{air,max}}\left(1 - \frac{3}{\pi}\theta\right) + \frac{1}{R_{air,min}}\left(\frac{3}{\pi}\theta\right) \tag{17}$$

$$\text{If } \theta\epsilon\left[0,\frac{\pi}{3}\right] \Rightarrow Y_{air}(\theta) = \frac{1}{R_{air,max}}\left(\frac{3}{\pi}\theta - 1\right) + \frac{1}{R_{air,min}}\left(2 - \frac{3}{\pi}\theta\right) \tag{18}$$

The magnetic co-energy, W_m^c, and energy, W_m, are symmetrical, expressions (19). The magnetic energy stored in the system is a rather difficult variable to obtain, since the flux linkage, Ψ, will have to be used as an independent variable and the current dependent of it. The magnetic co-energy, expression (20), even though, having no physically meaning, it's only the means towards a goal.

$$W_m(\theta,\Psi) = \int_0^{\Psi} i d\Psi \tag{19}$$

$$W_m^c(\theta,i) = \int_{i_0}^{i} \Psi di \tag{20}$$

The co-energy will have the flux linkage dependent on the current, since the current can be directly measured. The presence of magnets in the system will result in the need to have an imaginary current, i_0 (21), guaranteeing the complete demagnetization of the system for t=0.

$$i_0 = -\frac{B_r l_m}{2N\mu_m} \tag{21}$$

The flux linkage is directly dependent on the value of the flux (22), therefore in order to have the value of the flux in the system, (14) will be used. As it can be observed in (14) the each value of the flux will be dependent on two different currents, however it will be assumed all windings to be connected in series, making all currents equal.

$$\Psi(\theta,i) = N\phi(\theta,i) = N\,\frac{\frac{B_r l_m}{\mu_m} + 2Ni}{3R_{air}(\theta) + \frac{l_m}{\mu_m S_m}} \tag{22}$$

By applying (20) to the now known expression for the flux leakage (22), will give out the equation for the magnetic co-energy (23):

$$W_m^c(\theta,i) = \frac{(Ni)^2 + (Ni)\frac{B_r l_m}{\mu_m} + \left(\frac{B_r l_m}{2\mu_m}\right)^2}{3R_{air}(\theta) + \frac{l_m}{\mu_m S_m}} \tag{23}$$

Table 1 withholds the assumed values of the variables for the magnetic circuit modelling:

Table 1- Relevant characteristic of the proposed model geometry

Stator's Outer diameter	64 mm
Stator's inner diameter	50 mm
Stator's pole diameter	34 mm
Rotor outer diameter	32 mm
Rotor inner diameter	16 mm
Magnet length, $\mathbf{l_m}$	5.6 mm
Machine depth, L	20 mm
Remanence Magnetic field, $\mathbf{B_r}$	1.4 T
Number of turns in a winding, N	N
Max Air-gap, $\mathbf{g_{max}}$	16 mm
Min Air-gap, $\mathbf{g_{min}}$	1 mm
Frequency, $\mathbf{f}$	50 Hz
Magnet's magnetic permeance, $\boldsymbol{\mu_m}$	$1.05 * 4\pi 10^{-7}$
Air's magnetic permeance, $\boldsymbol{\mu_0}$	$4\pi 10^{-7}$

Assuming (22) was computed for only one winding turn and the current applied to the windings is null, we get the behaviour of the flux in the machine, taking only into account the magnets influence on the circuit, presented in Figure 11 - Flux in the top half of the machine, in a turn..

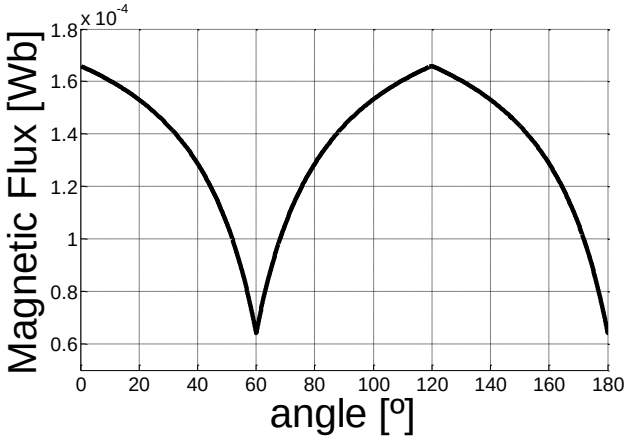

Figure 11 - Flux in the top half of the machine, in a turn.

Since the electromagnetic torque is the partial derivative of the magnetic co-energy, $W^{c}{}_{m}(\theta, i)$, for $i = cte$, and since no load is being applied to the system, it can be assumed the resulting torque as torque ripple.

$$T_{ri} = \left.\frac{\partial W_m^c(\theta, i)}{\partial \theta}\right|_{i=cte} = -3\frac{dR_{air}(\theta)}{d\theta}\frac{(Ni)^2 + (Ni)\frac{B_r l_m}{\mu_m} + \left(\frac{B_r l_m}{2\mu_m}\right)^2}{\left(3R_{air}(\theta) + \frac{l_m}{\mu_m S_m}\right)^2} \tag{24}$$

Even though angular position is an important variable when studying the machine in a stationary state, ultimately, in a rotation machine, angular speed, w, is one of the main characteristics. In an electric machine torque and electromotive force are directly related to the speed of the rotor. The only variable dependent of time is the angular position of the rotor, expression (25) shows this dependence:

$$\theta(t) = \theta_0 + w(t)t + \frac{a(t)}{2}t^2 \tag{25}$$

Once the equation for the angular position on the rotor is established, one can fully study the system at any given time. θ_0 represents the initial position of the rotor; w, the angular speed, this may be described with two different states: constant (26), transitory (27).

$$w(t) = \frac{d\theta}{dt} = \frac{2\pi}{T} = 2\pi f \tag{26}$$

The final variable will be the acceleration, $'a'$, this will be dependent on external variables since the rotor will spin due to external forces, considering the number of possibilities for it, it will stay as an open variable.

$$w(t) = w_0 + a(t)t \tag{27}$$

For the magnetic circuit study of the system, w will be assumed as described in (25) and the studied frequency for the rotation speed will be:

$$f = 50\ Hz \tag{28}$$

EMF in a winding appears when there is a variation of the flux passing perpendicular to it, the higher the variation rate the more EMF.

$$U_i = r_f i + \frac{d\Psi}{d\theta}\frac{d\theta}{dt} + \frac{d\Psi}{di}\frac{di}{dt} \tag{29}$$

In Figure 12, the full behaviour torque ripple (a) and the electromotive force (b) can be observed, for a full turn. To note, the magnetic circuit evaluation of the model was conducted considering all windings connected in series and no load attached to the machine, therefore the current are all the same and null.

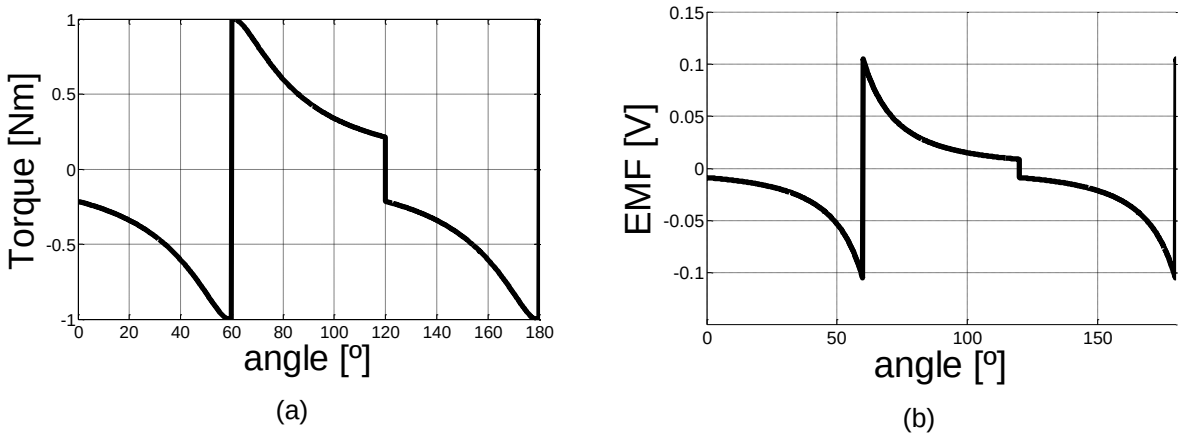

(a) (b)

Figure 12- (a) Torque on the top half of the machine, in a cycle; (b) EMF on the top half of the machine, for an one turn winding, in a cycle.

Figure 12 (a) shows a torque peak of $7.45 * 10^{-4}$ Nm, with a period of 120 mechanical degrees. The torques RMS is equal to $7.12 * 10^{-6}$ Nm and a variance of $2.90 * 10^{-9}$ Nm. Figure 12 (b) shows a voltage peak of 0.1 V per turn, with a period of 120 mechanical degrees. The EMF RMS is equal to $3.65 * 10^{-2}$ V per winding turn and a variance of $1.3 * 10^{-3}$ V. In Figure 12 (a), it can clearly be seen the torque ripple at no-load.

In order to obtain Figure 12 a magnetic circuit evaluation was made, consequently it can be observed some incoherencies between results and reality. Torque is a force, and to have it instantaneously change direction, would be required and infinite and instantaneous, this numerical discontinuity does not exist. This results appear only because no magnetic leakage was taken into consideration, if it was we would observe a smoother transition between its peaks and the spikes wouldn't exist.

2.2.2 Finite elements modulation of the 2D magnetic circuit model

In order to evaluate how significant, magnetic flux dispersion and magnetic saturation are to our model, a 2D distributed parameters study was implemented in a FEM. The 2D geometry, for half of the machine, is the one in Figure 13. In it, the cross sections were the magnetic flux was calculated are indicated by S_1, S_2 and S_3, and the dimensions of the model are the same used in the magnetic circuit evaluation, The magnets are represented as the rectangles with direction arrows, showing the direction of the magnets push.

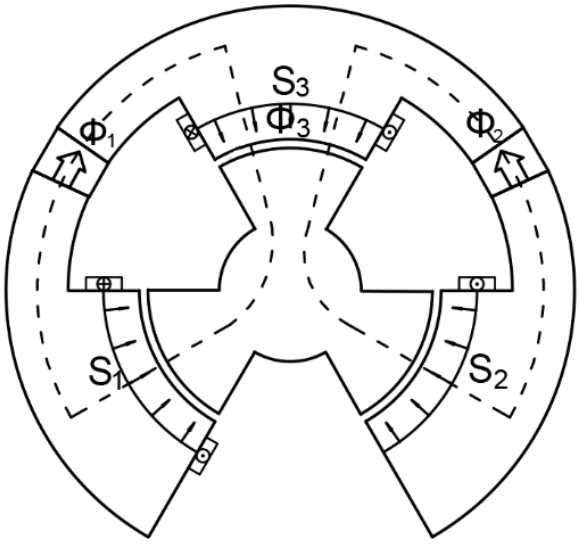

Figure 13 - Top half of the 2D machine model

Figure 14 shows the flux that passes through each cross section, of Figure 13. A series of static tests were made in order to obtain a more accurate view of the development of the fluxes and torque ripple of the model. A full turn has 360 steps, the study was made with no load, since the cogging torque, responsible for the ripple, is due to the presence of permanent magnets, in order to study it, only the influence of the permanent magnets was taken into account.

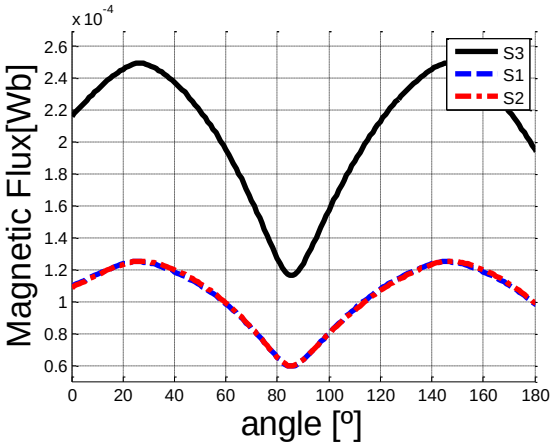

Figure 14 – Magnetic flux passing through S3, S1 and S2

The torque ripple occurs due to the reluctance torque. This torque is defined as the force applied by the system will trying to achieve equilibrium. Since the rotor is being forced to turn, due to an external force, once the rotor gets out of alignment, a force will appear pulling back the rotor to its original position. As soon as the rotor's pole starts getting near the next stator's pole, it will start pushing the rotor's pole towards himself, this new force will oppose the previous one, up to a point where one over shadows the other.

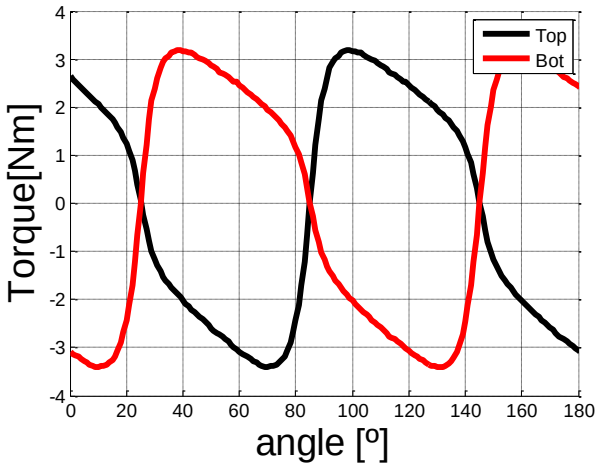

(a)

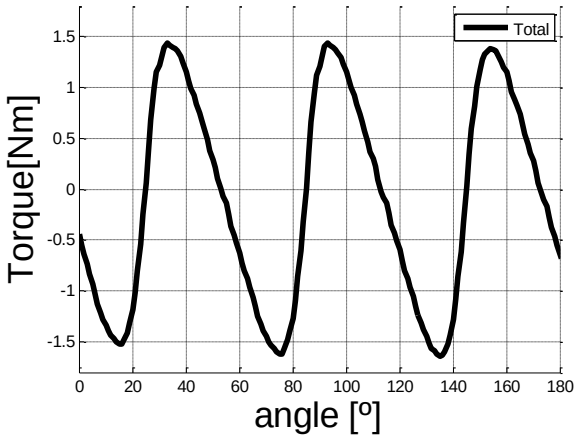

(b)

Figure 15- (a) torque produced by each stator piece of the machine; (b) predicted combined torque evolution of the machine.

Figure 15 (a) shows the torque at each stator piece independently and Figure 15 (b) the combination of the two. For Figure 15 (a) the resulting mean value were for curve 1 and 2, respectively: $-0.15\ \mathrm{Nm}, -0.14\ \mathrm{Nm}$; and the variance: $6.09\ \mathrm{Nm}, 6.15\ \mathrm{Nm}$.

Figure 15 (b) shows the final torque when the two stators are summed. There is an average torque of: $-0.30\ \mathrm{Nm}$; and the variance: $0.975265\ \mathrm{Nm}$. Even though the mean value increased the variance plummeted 84%, when compared with Figure 15 (a).

The expected effects of the different stators in the rotor are explicit in Figure 15 (a). One of the expected effects is the strengthening of the force applied to the rotor, whilst the air-gap gets narrower.

Another effect to notice is the deviation of the stators, the torque applied will be sum of the two waves in (a), expressed in (b) as a signal with twice the oscillation rate but with less than half the magnitude.

2.3 Analyses of the Flux-Switching Permanent-Magnet 3 legs Stator Electric Machine with 3D Magnetic Flow

The design for this new 3D magnetic FSM was based on the premise that combining the capability of the magnetic 2D machine studied in the previews chapter to reduce the torque ripple and maximization of flux variation by forcing it to flow through a common rotor piece. The proposed FSM is presented in Figure 16 (a) where it can be seen that it has a common stator but two separate rotor pieces. An expanded version of Figure 16 (a), Figure 16 (b) shows the PMs located in each stator piece and their respective magnetizing direction. Figure 16 (c) illustrates two poles arrangements for the stator windings in concentrated coils.

For electromechanical power conversion, the magnetic flux that goes through each coil, according to the angle deviation, θ, between the rotor and stator, will vary with the magnetic reluctance of its closed path. Since there are two different and opposing phase coils for the magnetic reluctance of the air-gap, one on the top and the other on the bottom, as shown in Figure 16 (c), there will be higher variation rate of flux.

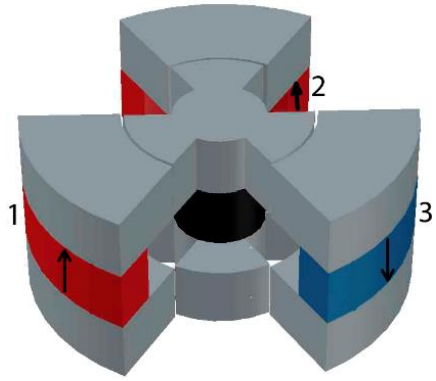

(a)

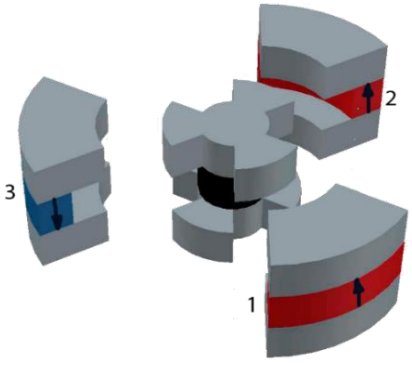

(b)

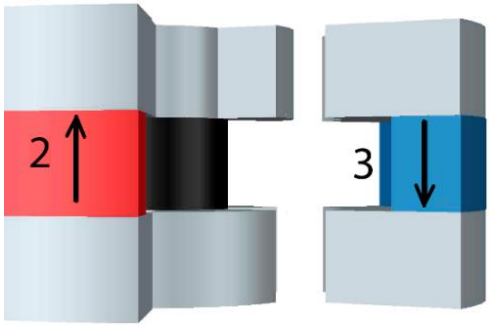

(c)

Figure 16-(a) proposed geometry for the 3D adaptation; (b) expanded view of the 3D model; (c) lateral view of the 3D model.

2.3.1 Analyses of the magnetic circuit

In this study, magnetic leakage was not taken into account, the magnetic permeance of the iron was considered too great, compared with air and the permanent magnet, and the magnetic flux is uniformly distributed on every cross session of the magnetic circuit. Also, each leg of the stator has the same dimensions and the top part of the rotor is equal to the bottom one, separated by a no magnetic material.

This simplified version was obtain by applying Ampere's law on the closed paths of the model, magnets 1 and 2 have their polarization turned upside down when compared to magnet 3. To note, all magnets have the same characteristics and every leg of the stator is similar. The air-gaps magnetic reluctance for the top layer is similar to the one in the bottom layer, differing only in terms of angle's phase. The effect of the two rotors in magnetic reluctance is the same as in the previous design.

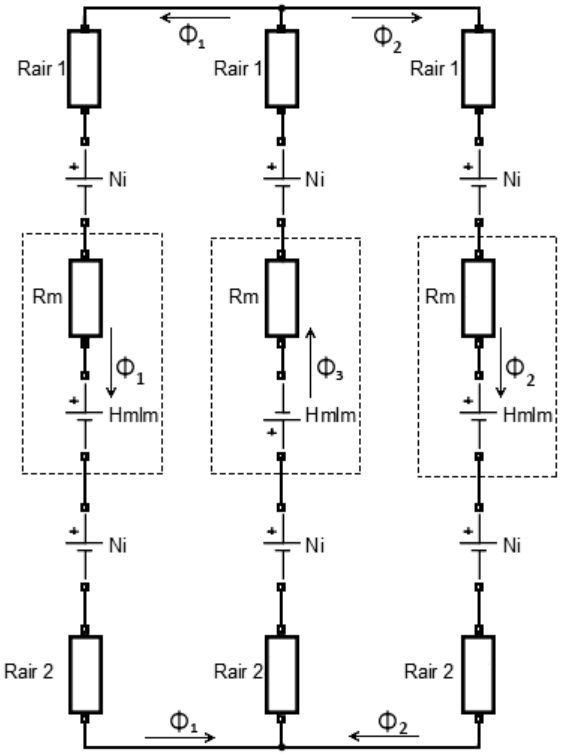

Figure 17 – Magnetic circuit representation for the design

By applying the principal of (8) and (9), there can be obtain a mathematical description of the model. Just like the previous design, this one, was considered to have all windings in series, therefore the current in assumed as i and constant. In this case R_{air1} and R_{air2} are respectfully the magnetic reluctance of the air-gap between top rotor and stator and the between the bottom rotor and the stator. l_m is the length of the magnets, S_m its cross section and μ_m the magnetic permeance. ϕ_1, ϕ_2 and ϕ_3 are the fluxes passing in each leg of the stator.

$$\begin{bmatrix} 2R_{air1}(\theta) + 2R_{air2}(\theta) + \frac{l_m}{\mu_m S_m} & R_{air1}(\theta) + R_{air2}(\theta) \\ R_{air1}(\theta) + R_{air2}(\theta) & 2R_{air1}(\theta) + 2R_{air2}(\theta) + \frac{l_m}{\mu_m S_m} \\ 1 & 1 \end{bmatrix} \begin{bmatrix} \phi_1 \\ \phi_2 \end{bmatrix} = \begin{bmatrix} 4Ni(t) + 2\frac{B_R l_m}{\mu_m} \\ 4Ni(t) + 2\frac{B_R l_m}{\mu_m} \\ \phi_3 \end{bmatrix} \quad (30)$$

Again, the air reluctance will vary with θ between its minimum and maximum values and to simplify it, $R_{air}(\theta)$ is inversely related with θ. The behaviour of the magnetic permeance of the air-gap, in this design, is on pair with the previous model. Therefore considering (31) and (32) as a representation of the magnetic permeance in the top air-gap is an accurate assumption:

$$\text{If } \theta \epsilon \left[0, \frac{\pi}{3}\right] \Rightarrow Y_{air1}(\theta) = \frac{1}{R_{air,max}}\left(\frac{3}{\pi}\theta\right) + \frac{1}{R_{air,min}}\left(1 - \frac{3}{\pi}\theta\right) \quad (31)$$

$$\text{If } \theta \epsilon \left[\frac{\pi}{3}, \frac{2\pi}{3}\right] \Rightarrow Y_{air1}(\theta) = \frac{1}{R_{air,max}}\left(2 - \frac{3}{\pi}\theta\right) + \frac{1}{R_{air,min}}\left(\frac{3}{\pi}\theta - 1\right) \quad (32)$$

In order to obtain the magnetic flux leakage, ϕ dependent on θ, it will be assume, as mention above, there is symmetry in the design, all legs of the stator are geometrically equal, except for the magnet's polarization, and the rotors have no difference.

$$\Psi(\theta, i) = N\phi(\theta, i) = \frac{2N}{3} \frac{\frac{B_R l_m}{\mu_m} + 2Ni(t)}{\frac{l_m}{\mu_m S_m} + R_{air1}(\theta) + R_{air2}(\theta)} \quad (33)$$

Applying (20) to the expression of the flux leakage in this model (33), the resulting equation, serves as a fairly accurate resource to obtain the magnetic co-energy (34):

$$W_m^c(\theta, i) = \frac{2}{3} \frac{(Ni)^2 + (Ni)\frac{B_r l_m}{\mu_m} + \left(\frac{B_r l_m}{2\mu_m}\right)^2}{\frac{l_m}{\mu_m S_m} + R_{air1}(\theta) + R_{air2}(\theta)} \quad (34)$$

By using the same premise as for the previous model, expression (24), on (34) we will extrapolate expression (35). This new formula allows us, not only to have a sense of the influence the magnets, current, number of turn in the windings and magnetic reluctance in the torque, but also to have a better understanding of the speeds influence in the torque ripple.

$$T_{ri}(\theta) = \left.\frac{\partial W_m^c(\theta, i)}{\partial \theta}\right|_{i=cte} = -\frac{2}{3}\frac{d\left(R_{air1}(\theta) + R_{air2}(\theta)\right)}{d\theta}\frac{(Ni)^2 + (Ni)\frac{B_r l_m}{\mu_m} + \left(\frac{B_r l_m}{2\mu_m}\right)^2}{\left(\frac{l_m}{\mu_m S_m} + R_{air1}(\theta) + R_{air2}(\theta)\right)^2} \quad (35)$$

2.3.2 Results of the analyses of the magnetic circuit

Figure 18 represents the results for the simulation: in (a) it can be seen the reluctance of the circuit through time; (b) represents the flux in the one of the legs with upward magnetic flow; (c) the wave form of the EMF available in the machine; (d) torque applied to the rotor in a turn.

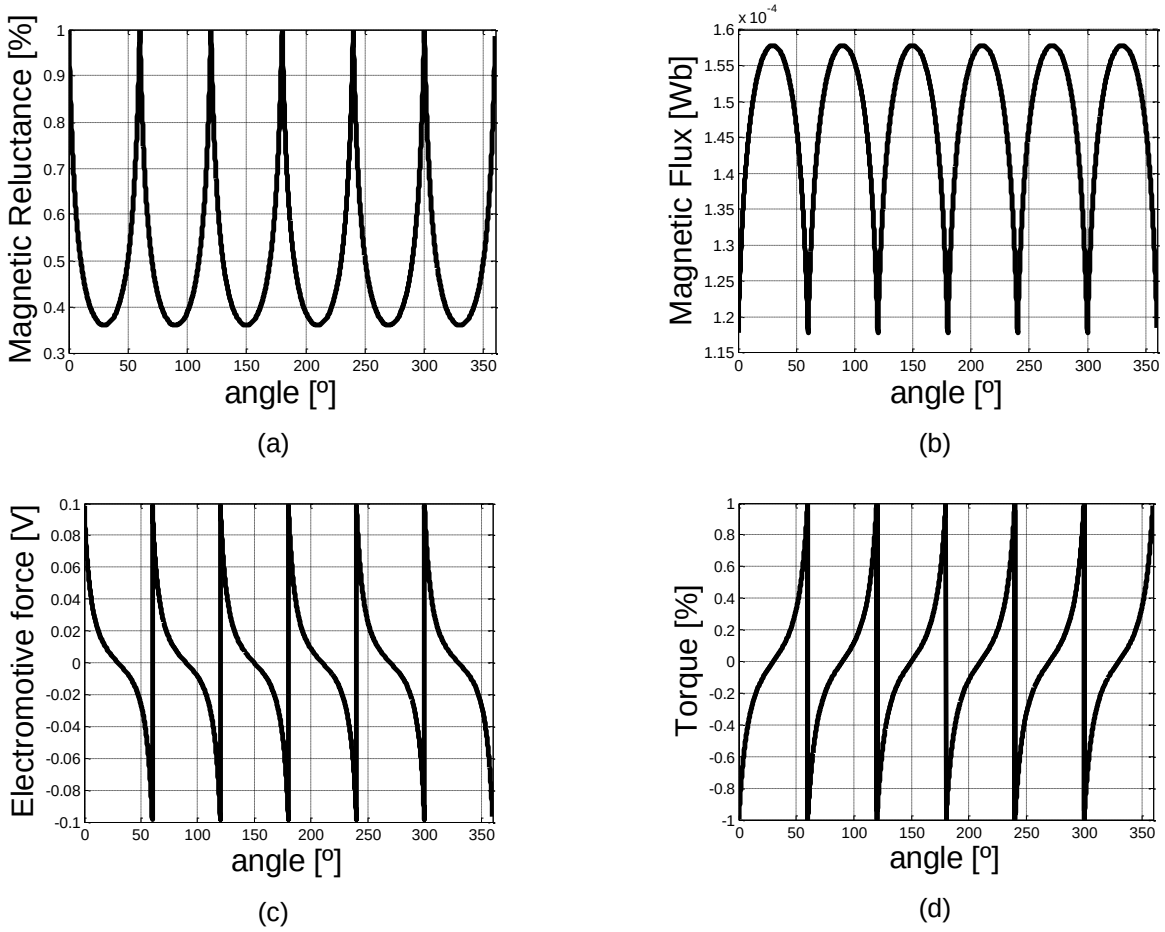

Figure 18- (a) combined magnetic reluctance of both air-gaps; (b) Magnetic flux, in a full turn; (c) Electromotive force, per winding turn, in a full mechanical turn; (d) Torque, in a full mechanical turn.

In Figure 18 (c) it can be seen the voltage peak is 0.1V with a period of 60 mechanical degrees, half of what the previous model was. The torques RMS is equal to $1.90 * 10^{-4}$ Nm and a variance of $6.30 * 10^{-10}$ Nm. The voltage RMS is $3.36 * 10^{-6}$ V, this experienced an 8% decrease, when compared to the previous one and a variance of $1.1 * 10^{-3}$ V. Should be noted, the asymmetry in the flux dispersion, this will result, as in the previous model, in an increased concentration of flux in one of the legs of the stator and rotors pole. Due to one of the poles having twice as much flux as any of the others, the force applied to that

pole will have a substantial influence in the torque ripple. On another note, once the magnetic saturation of the iron is taken in to consideration, this phenomena may result in an increased power loss.

2.4 Analyses of the Flux-Switching Permanent-Magnet 4 Legs Stator Electric Machine with 3D Magnetic Circuit

In this new study, the main objective was to get a better usage of the iron core and permanent magnets. A forth leg was added to the stator, as shown in Figure 19 (a), with each leg's iron volume and associated volume magnet decreased, since the overall dimensions remained. With this new design, more magnetic flux passes through each stator leg, also resulting in a symmetric flux distribution, hence a symmetric torque distribution around the rotor.

This new design shares almost all magnetic characteristics of the one described in segment 2.3. Aside from the extra leg, all magnetic material are the same. Each concentrated winding is placed in the stator, nearest to its edges, as shown in Figure 19 (b). The rotor pieces are separated by a non-ferromagnetic material, each stator and rotor pole will now be 45º. This geometry allows the flux to equally divide it self among all poles, avoiding the asymmetrical electromagnetic forces presented in the previous model and also the magnetic saturation.

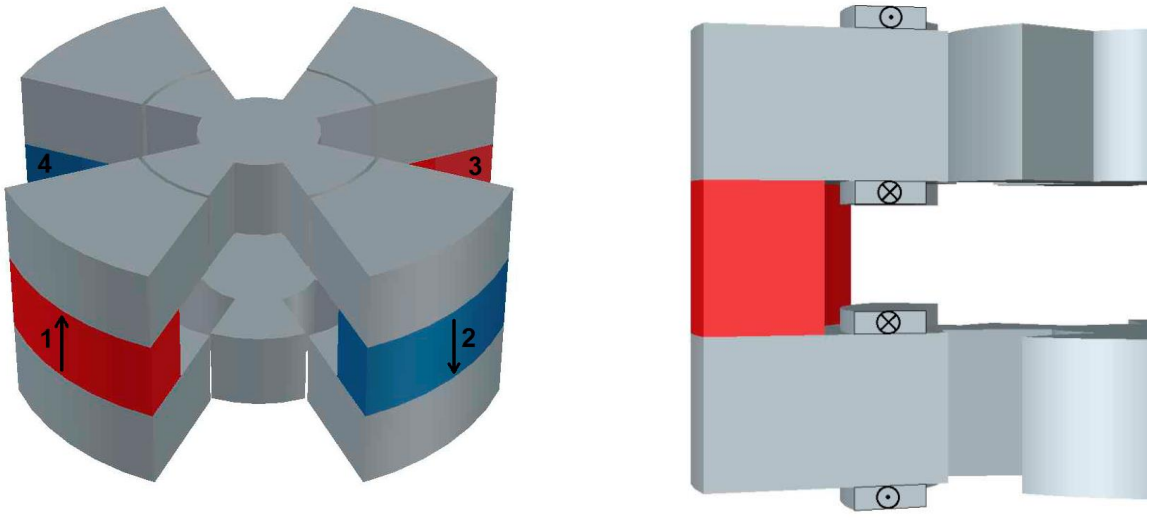

(a) (b)

Figure 19 – Proposed 4 legs common stator with a bi-partitioned rotor geometry; (b) one stator leg, winding direction.

2.4.1 Analyses of the magnetic circuit

Figure 19 showed a simplified view of the 4 legs design. Just like in the previous magnetic circuit, no magnetic leakage was taken into account, the magnetic permeance of the iron was considered to have a high value. The magnetic flux is evenly distributed on every session of the circuit, each leg of the stator has the same dimensions and the top part of the rotor is a copy of the bottom one, separated by a non-magnetic material, to be coupled. All concentrated windings are connected in series, meaning the current in equal all around the model.

By observing Figure 19, a representation of the machine's magnetic circuit can be effectuated as described in Figure 20. Both, this model and the previous one, share some similarities, being the only difference the added leg. Basing the study for the new magnetic circuit in magnetic flux conservation (8) and Ampere's law (9), using them in Figure 20, one can deduce:

$$\phi_1 = \phi_2 = \phi_3 = \phi_4 = \phi \tag{36}$$

$$R_{air1,max} = R_{air2,max} \tag{37}$$

$$R_{air1,min} = R_{air2,min} \tag{38}$$

$$R_{m1} = R_{m2} = R_{m3} = R_{m4} = R_m \tag{39}$$

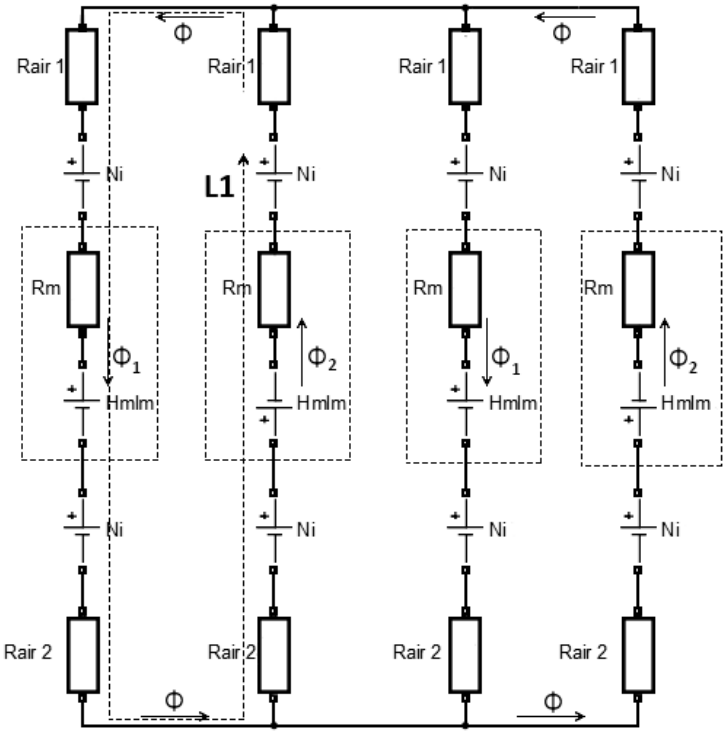

Figure 20- Proposed 4 legs model's magnetic circuit

Due to the symmetrical characteristics of the magnetic circuit and in order to simplify the model, the magnetic flux can be analysed using only two opposing legs, since all fluxes, ϕ_1 and ϕ_2, are equal no information will be lost. Expression (40) formulates using the magnetic circuit equivalent of the Kirchhoff voltage law applied to loop L1 shown in Figure 20. The influence of the rotor angle will have in the magnetic flux through the machine. Remember that all coils are series connected, thus the term $4\mathrm{Ni(t)}$ in (40).

$$\begin{bmatrix} \frac{l_m}{\mu_m S_m} + R_{air1}(\theta) + R_{air2}(\theta) & \frac{l_m}{\mu_m S_m} + R_{air1}(\theta) + R_{air2}(\theta) \\ 1 & -1 \end{bmatrix} \begin{bmatrix} \phi_1 \\ \phi_2 \end{bmatrix} = \begin{bmatrix} 4\mathrm{Ni(t)} + 2\frac{B_R l_m}{\mu_m} \\ 0 \end{bmatrix} \tag{40}$$

Again, as explained in section 2.1, the air-gap reluctance will change with θ between minimum and maximum values and for simplification, $R_{air}(\theta)$ is inversely related with θ, therefore considering (41) and (42) for the magnetic permeance of the top air-gap;

$$\text{If } \theta \epsilon \left[0, \frac{\pi}{4}\right] \Rightarrow Y_{air1}(\theta) = \frac{1}{R_{air,max}}\left(1 - \frac{4}{\pi}\theta\right) + \frac{1}{R_{air,min}}\left(\frac{4}{\pi}\theta\right) \tag{41}$$

$$\text{If } \theta \epsilon \left[\frac{\pi}{4}, \frac{\pi}{2}\right] \Rightarrow Y_{air1}(\theta) = \frac{1}{R_{air,max}}\left(\frac{4}{\pi}\theta - 1\right) + \frac{1}{R_{air,min}}\left(\frac{4}{\pi}\theta - 2\right) \tag{42}$$

The bottom air-gap, denoted 2, will be defined in a similar away by expression (43) and (44):

$$\text{If } \theta \epsilon \left[0, \frac{\pi}{4}\right] \Rightarrow Y_{air2}(\theta) = \frac{1}{R_{air,max}}\left(\frac{4}{\pi}\theta\right) + \frac{1}{R_{air,min}}\left(1 - \frac{4}{\pi}\theta\right) \tag{43}$$

$$\text{If } \theta \epsilon \left[\frac{\pi}{4}, \frac{\pi}{2}\right] \Rightarrow Y_{air2}(\theta) = \frac{1}{R_{air,max}}\left(2 - \frac{4}{\pi}\theta\right) + \frac{1}{R_{air,min}}\left(\frac{4}{\pi}\theta - 1\right) \tag{44}$$

Substituting (36) in equation (40) given the total magnetic flux linkage by the four electric circuits and expressed by (45).

$$\Psi(\theta, i) = N\phi(\theta, i) = N\left(\frac{\frac{B_R l_m}{\mu_m}}{\frac{l_m}{\mu_m S_m} + R_{air1}(\theta) + R_{air2}(\theta)}\right) + N^2\left(\frac{2i}{\frac{l_m}{\mu_m S_m} + R_{air1}(\theta) + R_{air2}(\theta)}\right) \tag{45}$$

As explained in section 2.2.1, applying (20) to the expression of the magnetic flux linkage in this model (45), and the resulting equation for the magnetic co-energy becomes given by (49).

$$W^c_{m_{bobine}}(\theta, i) = \frac{(Ni)^2}{\frac{l_m}{\mu_m S_m} + R_{air1}(\theta) + R_{air2}(\theta)} \tag{46}$$

$$W_{m_{magnet}}^{c}(\theta, i) = \frac{\left(\frac{B_r l_m}{2\mu_m}\right)^2}{\frac{l_m}{\mu_m S_m} + R_{air1}(\theta) + R_{air2}(\theta)} \tag{47}$$

$$W_{m_{mutua}}^{c}(\theta, i) = \frac{(Ni)\frac{B_r l_m}{\mu_m}}{\frac{l_m}{\mu_m S_m} + R_{air1}(\theta) + R_{air2}(\theta)} \tag{48}$$

$$W_m^c(\theta, i) = W_{m_{bobine}}^{c}(\theta, i) + W_{m_{magnet}}^{c}(\theta, i) + W_{m_{mutua}}^{c}(\theta, i) \tag{49}$$

By using the same premise as in 2.2.1, substituting in expressions (24), the equation for magnetic co-energy with (49) will result in (50). As in that section, the influence of the magnets, current, number of turns in the windings, the magnetic reluctance and speed on the torque is analysed.

$$T_{ri}(\theta) = \left.\frac{\partial W_m^c(\theta, i)}{\partial \theta}\right|_{i=cte} \Leftrightarrow$$

$$\Leftrightarrow T_{ri}(\theta) = -\frac{d\left(R_{air1}(\theta) + R_{air2}(\theta)\right)}{d\theta} \frac{(Ni)^2 + (Ni)\frac{B_r l_m}{\mu_m} + \left(\frac{B_r l_m}{2\mu_m}\right)^2}{\left(\frac{l_m}{\mu_m S_m} + R_{air1}(\theta) + R_{air2}(\theta)\right)^2} \tag{50}$$

2.4.2 Results of the analyses of the magnetic circuit

In table 2, it can be found the geometric and NdFeB characteristics of the 3D machine. For this study, no electric load was considered. The results, for that reason, will only consider the magnets influence in the magnetic flux, EMF and torque.

Table 2 - 3D machine model for the four legs common stator

Stator's Outer diameter	64 mm
Stator's inner diameter	31 mm
Rotor outer diameter	30 mm
Rotor inner diameter	15 mm
Rotor and stators depth, per iron piece	20 mm
Magnets outer radios	32 mm
Magnets inner radios	25 mm
Magnets surface	156.69 mm^2
Magnets depth	10 mm
NdFeB	$B_r = 1.4\ T;\ H_c = 1114084\ A/m$

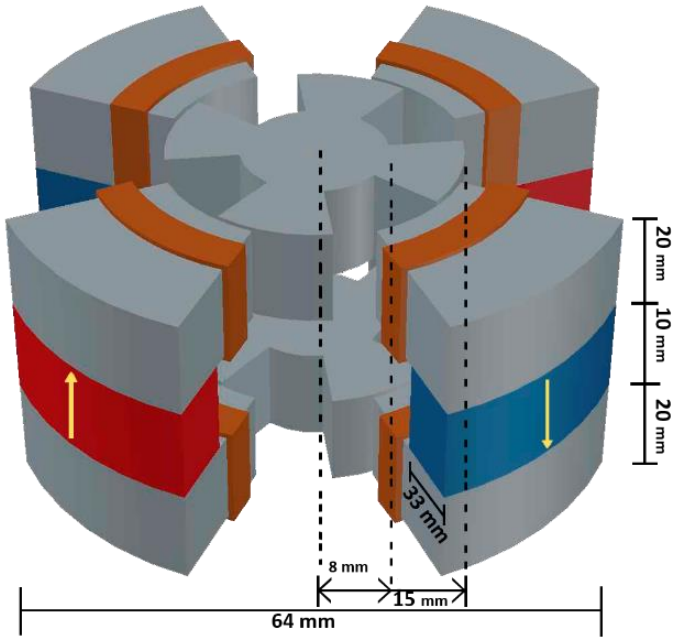

Figure 21 – 3D Machine model for the four legs common stator

Figure 22 shows the results for the simulation, using the model developed in previous section, Figure 21 using the dimensions in Table 2, with a rotation speed of 3000 rpm, each graph only represents the value of one leg: Figure 22 (a) it can be seen the magnetic reluctance evolution of a leg (two airgaps and one magnet) through one rotation; (b) represents the flux in the one of the legs; (c) the behaviour of the EMF per turn, per winding; being 0.15V its amplitude value and (d) generator's torque evolution during one turn. The voltage will be computed by (29).

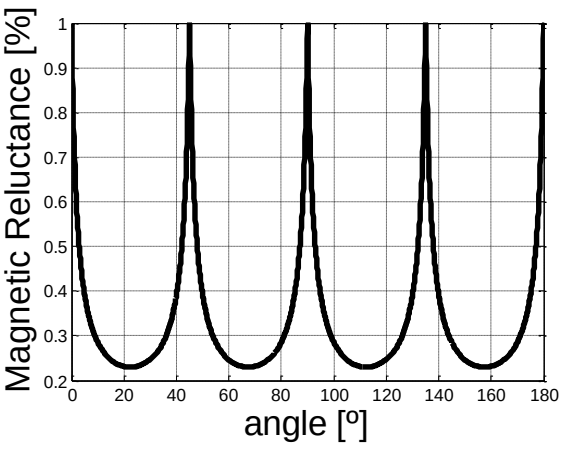

(a)

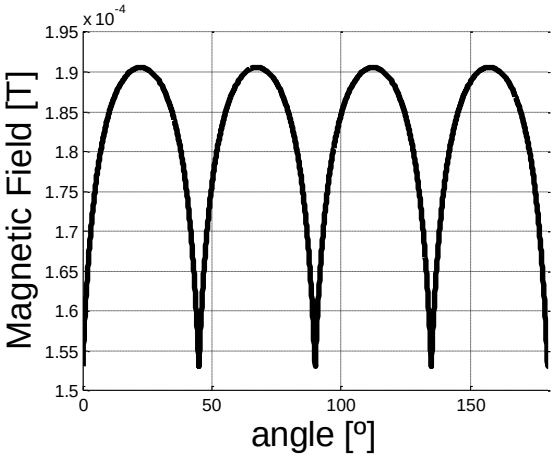

(b)

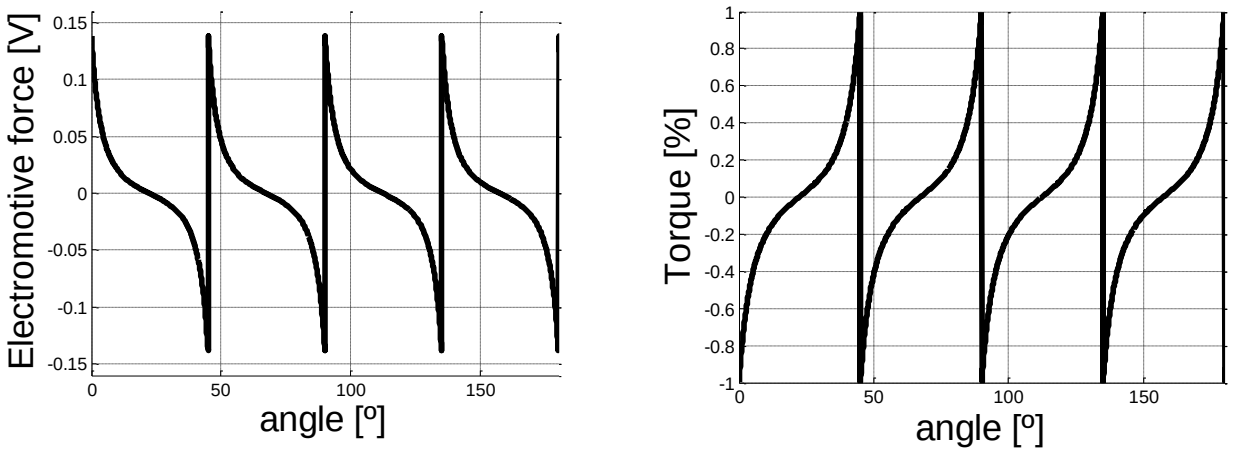

Figure 22 - (a) Evolution of magnetic reluctance during one rotation, (b) magnetic flux, (c) EMF, per winding turn; (d) Torque.

Compared to the machine studied in chapter 2.3, this one, due to its forth leg, has made the magnetic induction variation increase from six electric cycles per turn to eight cycles per turn, as shown in Figure 22 (b), also its value increased. As it can be seen in Figure 22 (c), the EMF pick and RMS increased around 50%.

Since the variation rate of the magnetic induction increased over 30%, resulting in the increased EMF, the new four legs design will be the one with the most promising results. The number of electric cycles per mechanical turn increased from 6 to 8, therefore the electric frequency of the magnetic flux raises, intensifying the EMF.

2.5 Material for the machine

The out of the box geometry presents limitations for the materials. Laminated iron in a machine that can be described in a frame, is highly beneficial, from high saturation point to small power losses. However for this topology, the use of laminated iron would greatly increase the magnetic reluctance of the machine. As indicated in Figure 23 (a) by pairs of bold arrows, the magnetic flux would have to force its way through the insulation between laminated plates. The insulation material has a magnetic permeance on par with air, causing the magnetic reluctance of the magnetic circuit to increase drastically.

Another approach would be to have the plates as seen in Figure 23 (b), this would solve the problem presented in the other configuration, of having the magnetic flux force its way through the insulation, however the cost of making such plates would increase the manufacturing cost of the machine. This configuration would also increase the power losses in the plates, due to induced currents in the iron, since the plates would have to get wider.

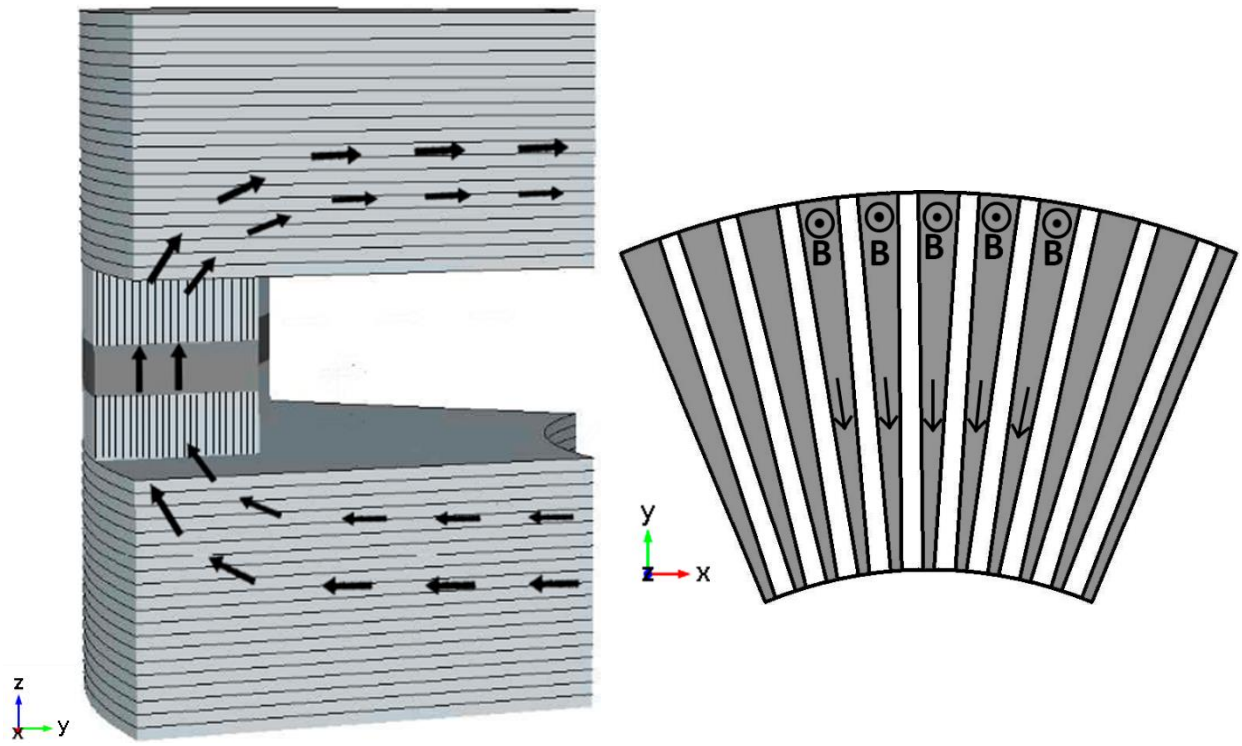

(a) (b)

Figure 23- 4 legs model: flux flow through one stator leg. Machine core construction using: (a) laminated plates x, y axis and laminated plates in the x, z axis; (b) laminated plates alternative configuration x, y view.

The proposed solution for the iron core is the using a soft iron composite magnetic material. This type of ferromagnetic material is characterized by “freedom of circulation” for the magnetic flux (isotropic property) and low power losses, since its electric conductivity is small. However, its isotropic property comes at a cost. In order to manufacture these materials, one must cover iron dust with a resin based material. Should be noted, since the rotor will not be subdued to flux trying to travel in the z axis, the can be made out of laminated iron, reducing the magnetic reluctance and increasing the saturation tolerance for this piece.

Figure 24 illustrates the soft iron composite material from a micro perspective. The circular shaped objects represent the iron particles, between them the resin, giving it consistency, and the arrow illustrate the small induced currents. The resin increases the magnetic reluctance of the material, around ten time of a regular laminated irons, this seemly great increase, is still insignificant when compared with the airs magnetic reluctance, or even with the one on the laminated iron when traveling perpendicular to the iron plates.

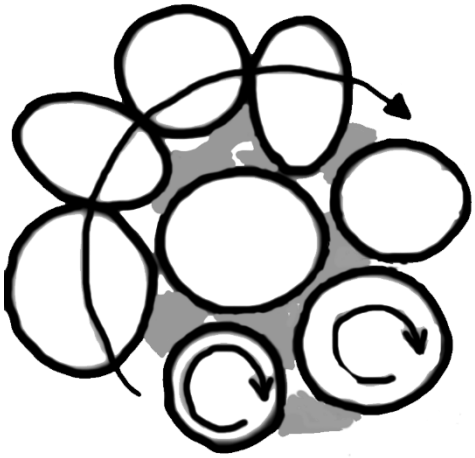

Figure 24- soft-iron composite, micro perspective

Soft iron composites have a lower saturation curve, making magnetic saturation a relevant concern for the model. Since the best and easiest way to control the magnetic flux is by altering the magnetic reluctance or the magneto motive force, therefore the best solution would be too change the magnets length.

According to the saturation curve of the ferromagnetic parts, Figure 25, an optimal solution for the magnetic flux density would be on the knee of the curve, as pointed out as zone 1 in the curve of Figure 25, since this region represents the maximum magnetic energy density.

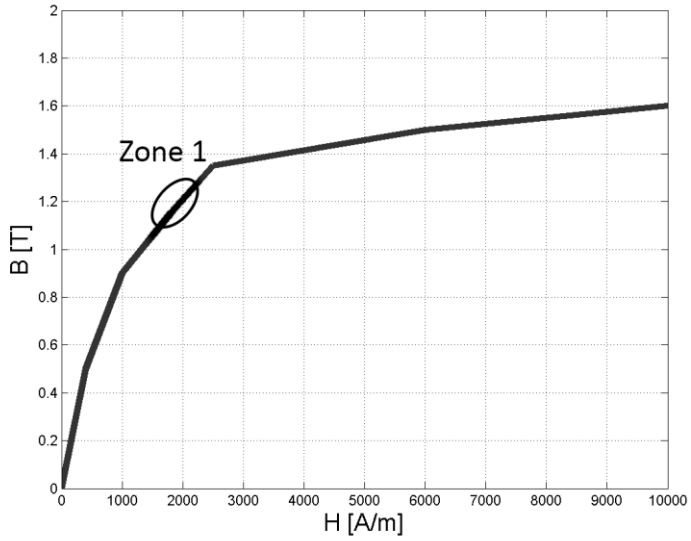

Figure 25- BH curve of the soft-iron composite used in the generator model.

As it can be seen the value for the magnetic field B would be approximately $1.2\,\mathrm{T}$ for an H around $2000\,\mathrm{A/m}$. At this value, the soft-iron has just barely started getting into the saturation zone. From

this point onward, the electromotive force would still increase. However, magnetic saturation will decrease the efficiency of the machine. Hence, keeping the maximum value of B around this value, it will be assured the best usable power per volume ratio.

Taking magnetic saturation in to consideration for the magnetic circuit evaluation done in the previous chapter and using the dimensions in Table 3, it was concluded that the magnetic field would reach a significant level of saturation, but only in the cross-section highlighted in red in Figure 26. In the winding region, marked in blue, this effect wouldn't be noticed, meaning its use is insignificant for this design when calculating the EMF, with no load.

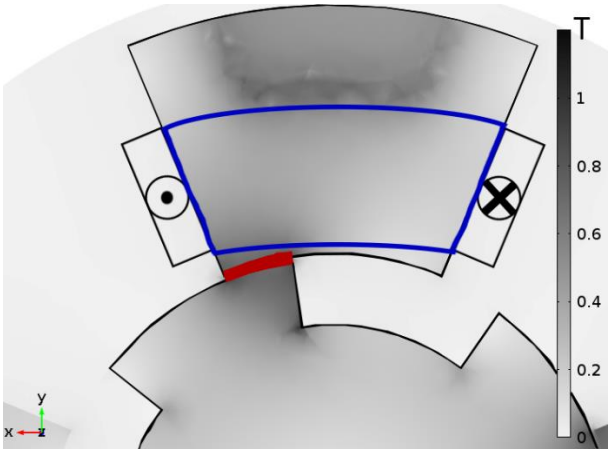

Figure 26- Model of the 4 legs common stator generator, highlighting relevant cross-sections for Figure 27: winding region marked in blue; cross-section connecting the rotor's pole with the stator in red.

Table 3- 3D model, 4 legs common stator

Stator's Outer radios	324 mm
Stator's inner radios	172 mm
Rotor outer radios	170 mm
Rotor inner radios	130 mm
Rotor and stators depth, per iron pieces	80 mm
Magnets outer radios	324 mm
Magnets inner radios	270 mm
Magnets cross-section	3200 mm^2
Magnets depth	4 mm
Magnet(NdFeB) parameters	B= 1.4 T; Hc= 1114084 A/m

The resulting induction magnetic field in the two different sections in a stator pole are the ones expressed in Figures 24 (a) and (b). In Figure 27 (a) and (b) it can be seen the behaviour of the magnetic field in the winding region, represented by the black line, this oscillation will be responsible for the

appearance of EMF; In Figure 27 (b) the red line represents the magnetic field in the cross-section connecting the rotor's pole with the stator, should be noted magnetic saturation was not taken into consideration.

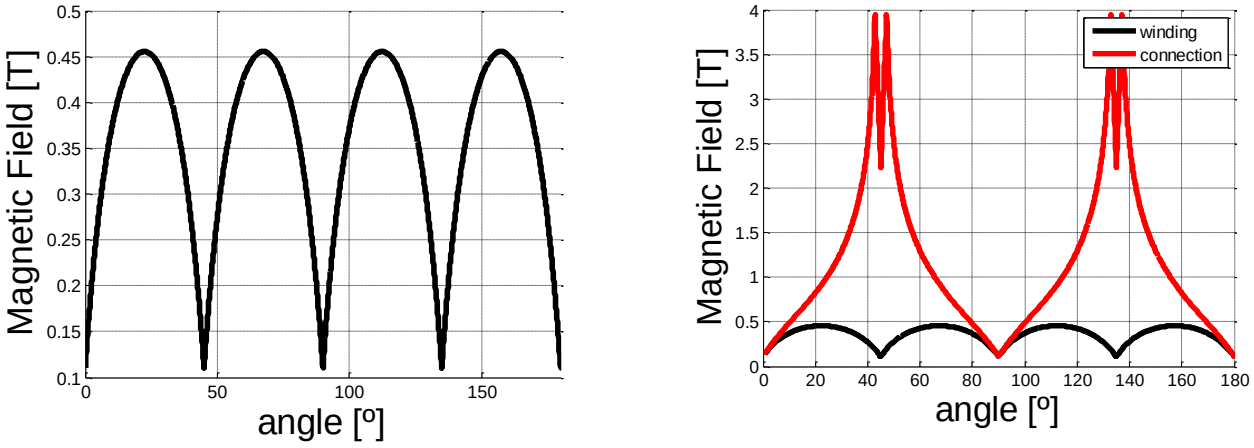

(a) (b)

Figure 27- (a) Magnetic field behaviour in the winding region; (b) comparison between the magnetic field in the winding region and on the connection between the rotor and the stator marked in Figure 26

The strongest magnetic field, in the winding region will occur when half the rotor pole is aligned with the stator. Even though the magnetic saturation in the winding region is none existing, at the end of the stator the same would not be true. Using the magnetic circuit study evaluation, therefore considering no magnetic dispersion and without taking saturation into account, the resulting magnetic field at the edge of the stator pole could be represented by the red line in Figure 27 (b). Since the value of the magnetic field greatly exceeds 1.2 T, it can be assumed, in a real case, there will not only be an increase in the magnetic reluctance of the circuit, as well as magnetic dispersion. These two effects will surely decrease the value of the induction magnetic field and also attenuate its share characteristics

2.6 Finite-element Analyses of the Flux-Switching Permanent-Magnet 4 Legs Common Stator Electric Machine with 3D Magnetic Flow

Due to the soft-iron composite be a material with a large electrical resistivity, induced currents in the soft iron pieces will not be accounted for. Using a scale from 0 to 1.2 T will allow us to spot issues in the magnetic flux distribution.

Figures 25 (a), (b) and (c) show, for three different rotor positions, $\theta = 0º, \theta = 45º$ and $\theta = 22º$ respectively, how the induction magnetic field is distributed in the rotor and stator pieces.

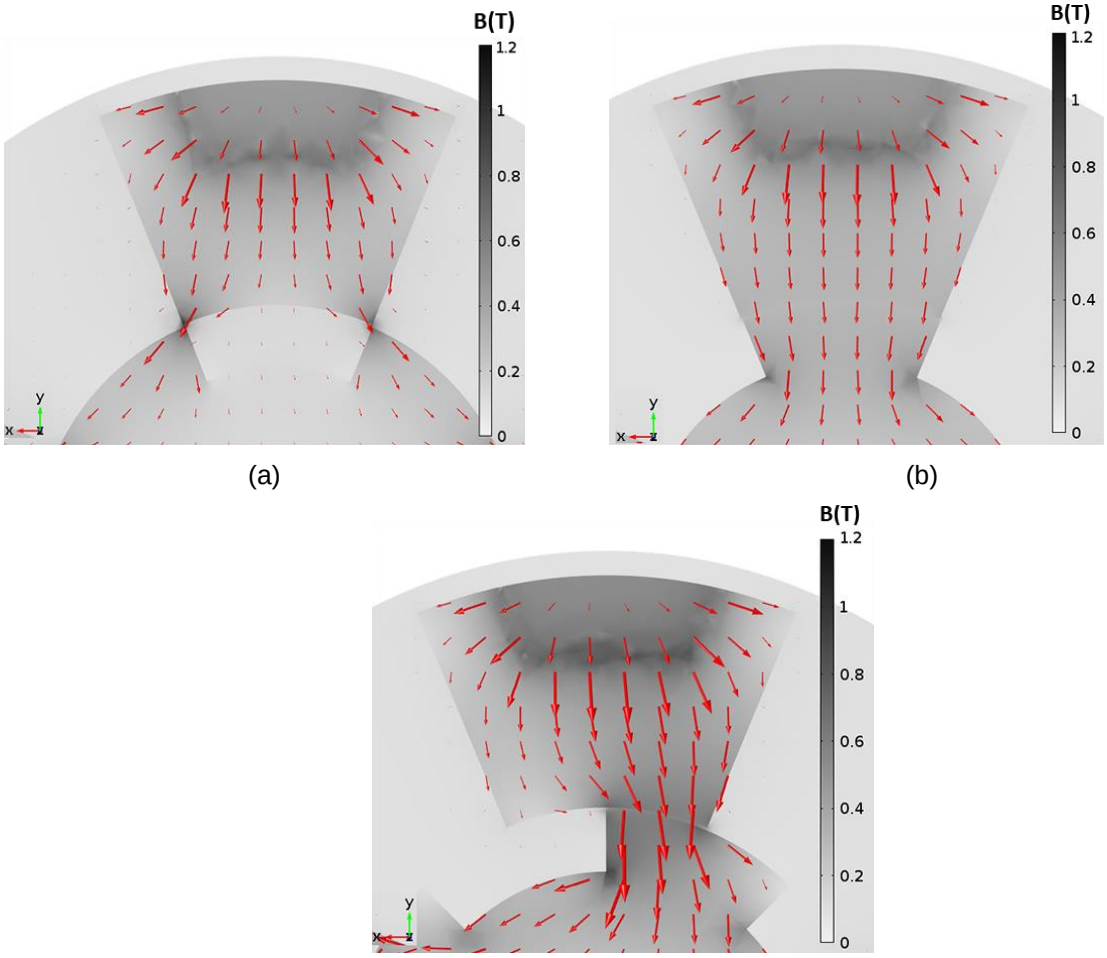

Figure 28- 4 legs common stator for different rotor positions and respective magnetic field distribution: (a) 0º; (b) 45º; (c) 22º.

Table 4 lists the magnetic flux value crossing section S, indicated in Figures 26 as the winding region. Positions 0º and 45º are those where the flux reaches a minimum value, as already illustrated by Figure 27 (a) as the minimum value of the magnetic induction field. Now, the maximum flux occurs around 22º, since in this region the magnetic reluctance is minimum, also predicted by the maximum field value, reached for this position in Figure 27 (a).

Table 4- Magnetic flux for different rotor positions

	0º	**Min(45º)**	**Max(22º)**
Magnetic Flux (mWb)	4.63	3.77	5.76

Figure 29 (a) and (b) show, for a speed of 3000 rpm and without load, the evolution of the magnetic flux passing through the top and bottom coils of a leg and the EMF induced per turn for each coil. Unlike the magnetic circuit study, the magnetic flux obtained by the 3D FEM, as half the frequency, due to difference in minimum values for the magnetic flux in the top and bottom windings, seen in Figure 29 (a). Considering

the two windings are connected in series, the resulting wave will not be affected by decreased in variation rate, as seen in Figure 30 (a).

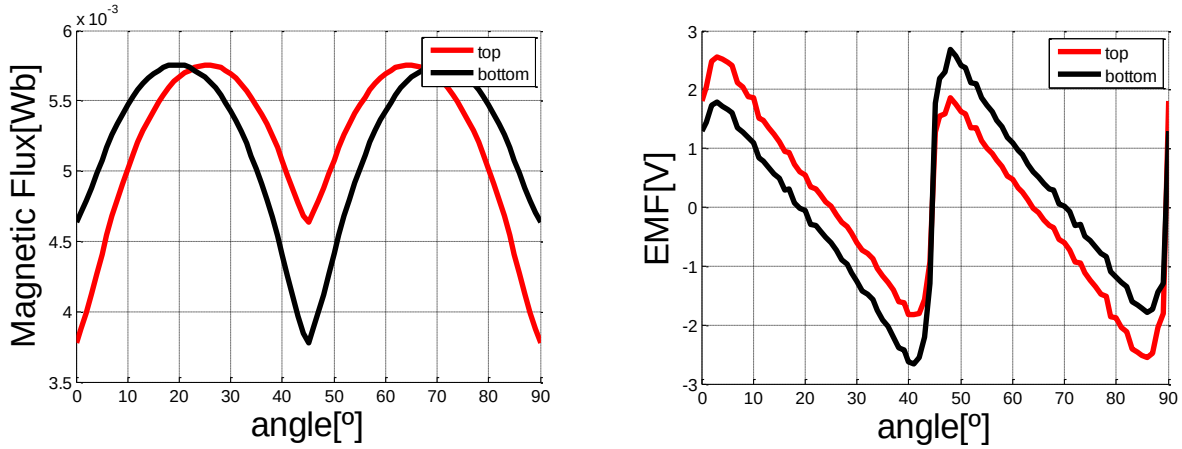

(a) (b)

Figure 29- (a) Magnetic Flux passing through the coils of a leg; (b) Resulting EMF in the respective windings, with no load and at 3000 rpm.

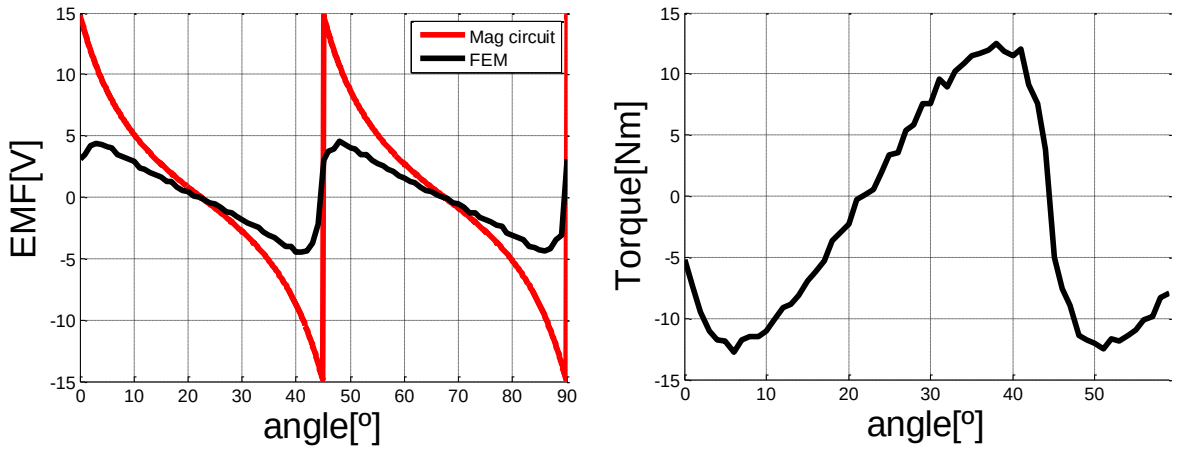

(a) (b)

Figure 30-(a) Resulting EMF of a leg at rpm 3000, with no electrical load; (b) torque of the model, no electrical load

Performing the same method as used for chapter 2.4.2, replacing the machine's dimensions with the ones used for the FEM, it was obtained the RMS for the EMF per turn leg.

Table 5- Root means square of the total EMF per turn leg and of the torque without electrical load

	EMF per turn(V)(magnetic circuit)	EMF/turn/leg(V)(FEM)	Torque(Nm)(FEM)
RMS	6.20	2.80	8.78

The EMF per turn reduced about 55%, this significant deficit comes as an obstacle. There is not sufficient generation of EMF which would result in misused magnetic energy. This occurs due to the lack of magnetic reluctance variation associated with the reduction of the torque ripple goal, little magnetic reluctance variation equals little magnetic power variation, resulting in little torque ripple.

From Figure 30 b) it is clear the behaviour of the torque ripple. This value could still be decreased but decreasing would also decrease the EMF, therefore one question remains, how can we have bigger flux variations, without increasing torque ripple?

A first hint comes from Figure 28 (c) where, not only was the flux mainly on one side of the stator pole, it didn't affect much the value of the magnetic flux passing. As we will see in the next chapter, utilising this knowledge and adapting the stator and rotor will vastly increase the EMF per turn of the machine.

3 Design adaptations in order to reduce torque ripple and maximize EMF per turn

As stated in the previous chapter, the last design, shown a significant decrease in EMF per turn, although achieving a reduced torque ripple. However, some questions remain: how to increase the EMF per turn? What if instead of having one arm per stator pole, there were two, as shown in Figure 31, with each arm having a coil? This would allow placing four coils per stator leg and to use the rotor's position to guide the flux through each coil. In Figure 31, Figure 32 and Figure 33, arrows were used to illustrate the expected path of the magnetic flux for each configuration. Since the main goal is to focus, at some rotor position, all magnetic flux on one of the stator's arm, this new design is more susceptible to cause magnetic saturation.

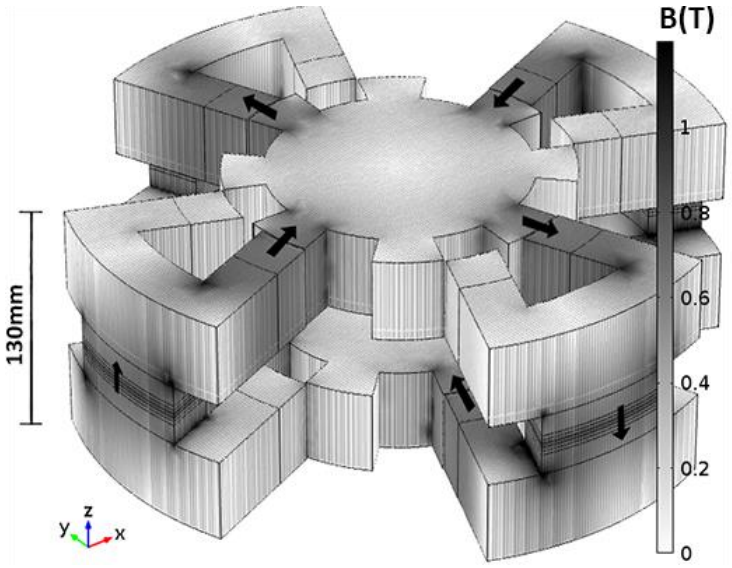

Figure 31- Two arms six legs stator, eight rotor salience

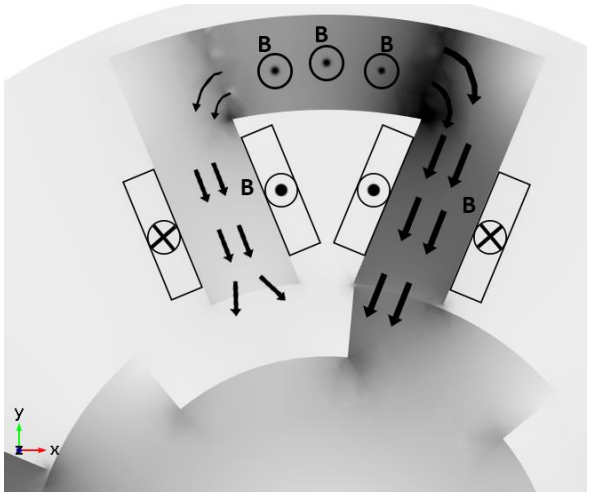

Figure 32- Divided common stator pole, 4 pole rotor, with winding placement and magnetic flux path

From Figure 32, the majority of the magnetic flux would flow through the right stators arm, choosing the one with the least magnetic reluctance. The left arm should have a significantly lower magnetic flux, since its magnetic reluctance of the arm increases significantly. This will increase the EMF per turn, but also the two arms will add a multiplying factor of two on the final EMF due to doubling the number of coils per stator piece.

3.1 Rotor adaptation to the new two-arms divided stator pole geometry

Since the stator's pole is now divided into two arms, each respective cross-section is significantly smaller. Knowing this, it could be beneficial to increase the number of rotor saliences from 4 to 8 to avoid any dead-zone, in the EMF's. Adding more than 8 would not benefit the design since the main goal, of dividing the stator, was to force the magnetic flux to choose only one of the arms, as seen in Figure 33.

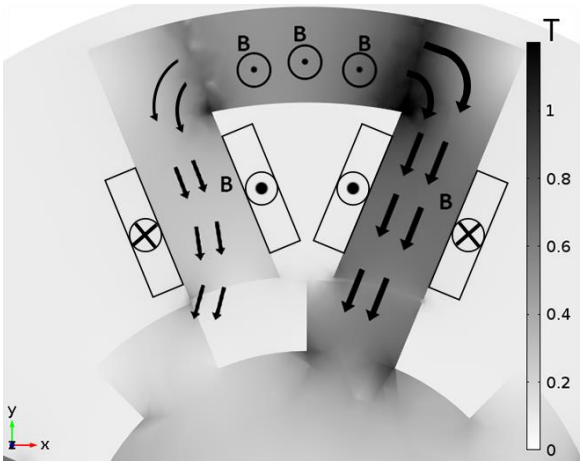

Figure 33- Two-arms common stator pole, 8 pole rotor, with winding placement and magnetic flux path.

Doubling the number of rotor poles from 4 to 8, it is expected to see an increase in each winding's EMF. Two opposing effects will take place: despite doubling the frequency, there is a decrease in the magnetic flux magnitude linked by each arm winding. The double frequency occurs due to the increased number of rotor poles. The magnetic flux magnitude decreases due to the proximity of the rotor poles, as seen in Figure 33 in the left arm.

Table 6- Magnetic flux difference for each model

	Min Flux (mWb)	Max Flux (mWb)	ΔFlux(mWb)
4 poles	0.89	4.66	3.77
8 poles	1.28	4.41	3.13

Figure 34 (a) and (b) explicitly show, respectfully, the evolution of the EMF per turn and per stator leg, and the resulting torque ripple with no load and with 3000 rpm speed, for 90º turn on the rotor.

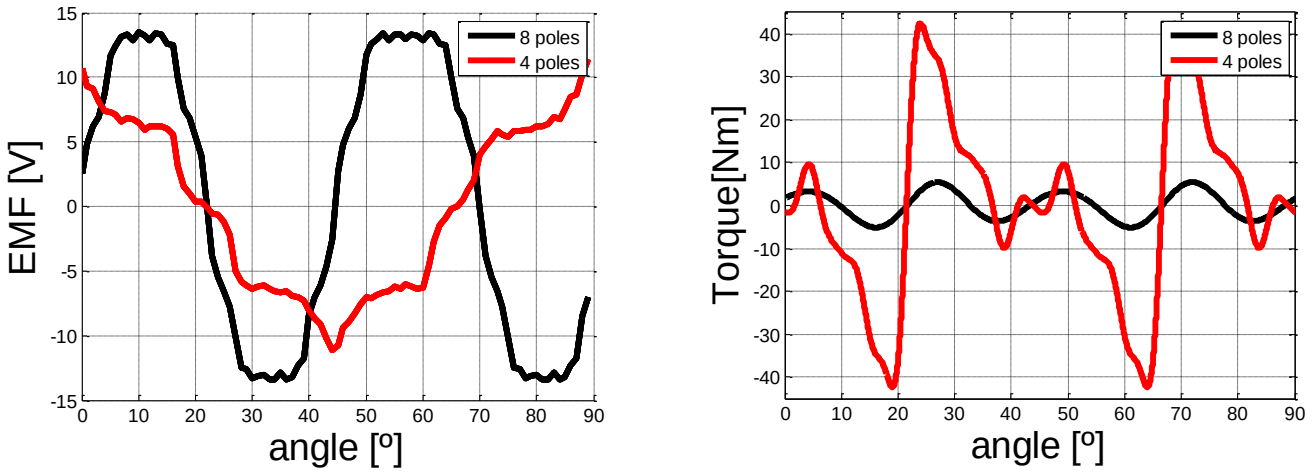

(a) (b)

Figure 34- (a) resulting EMF of each model, no load, 3000 rpm; (b) resulting torque of each model, no load.

Table 7 clearly shows how superior the 8 rotor salience configuration is compared with the 4 rotor salience one. Not only did the EMF increased around 64%, the torque ripple decreased by 85%.

Table 7- Comparison of the different models characteristics.

Model	EMF/turn(V)	Torque ripple (N.m)
chapter 2.6	2.80 (-56%)	8.78 (-57%)
4 poles	6.35	20.44
8 poles	10.48 (+64%)	3.16 (-85%)

The new stator configuration greatly increased the magnetic flux variation, but this also increased the magnetic energy variation, since the 4 pole rotor configuration was not optimal. This resulted in a significant increase in the torque ripple value when compared with the model from chapter 2.6 from 8.78 Nm to 20.44 Nm. However changing the rotor to 8 poles greatly decreases the torque value and increases EMF per turn per stator leg.

3.2 Stator adaptation to the two-arms divided stator pole with a 8 pole rotor poles

The two main concerns in this project are always keeping a balanced magnetic flux flow that not only prevents uneven magnetic saturation, but also keep an even distribution of mechanical forces responsible for torque ripple. Therefore, in order to have a better usage of the area around the rotor, an extra pair of stator legs could be added to the model, as seen in Figure 35. The general size of the machine was maintained to that of Figure 31. Each stator leg will be always linking to the up and down rotor piece. Hence, it is expected that the extra pair will greatly impact the EMF per turn without throwing the electric machine out of balance.

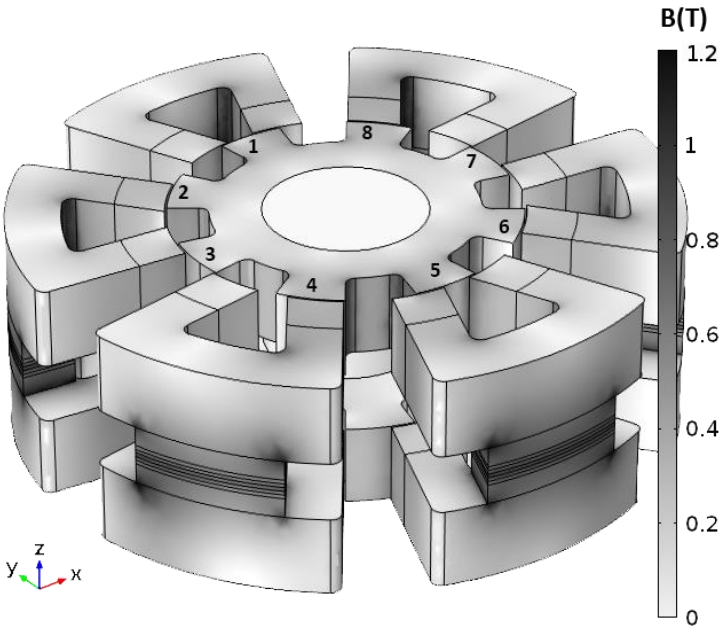

Figure 35- Proposed six stator legs distribution and its eight rotor saliences.

Just like before the main goals will be increasing the EMF per turn and decreasing torque ripple. Both models possess, for each leg, the same waveform, as supported by Figure 36 (a) which was obtain by calculating the change rate of the magnetic flux passing in each arm of a stator leg. On the other hand Figure 36 (b) supports the idea of a 50% increase in the torque ripple's frequency.

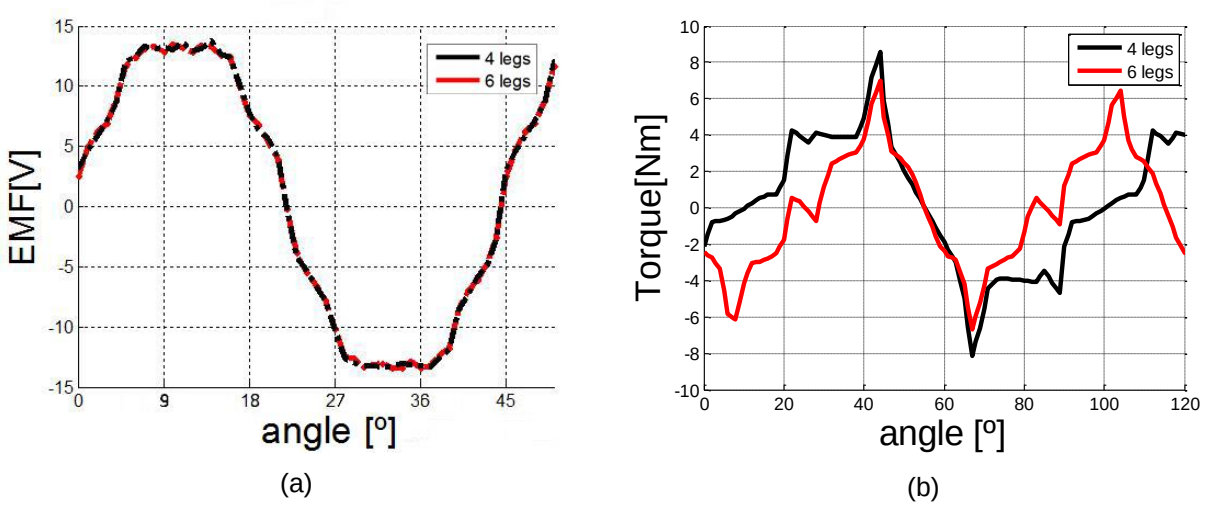

(a) (b)

Figure 36-Results from the 4 legs and 6 legs models, at 3000rpm and no electrical load: (a) EMF of a leg; (b) torque in a rotor salience.

Since the both results in Figure 36 are obtained through 3D FEM of the electric machine, all results are bound to have a numerical error associated with it due to the used mesh size. Therefore, in order to filter this error, it is advantageous to perform a FFT analysis of the signal, removing any harmonic with less than 5% significance when compared with the fundamental harmonic. Figure 37 demonstrate two examples of this procedure, in (a) for the EMF and in (b) for the torque of the 4 legs stator.

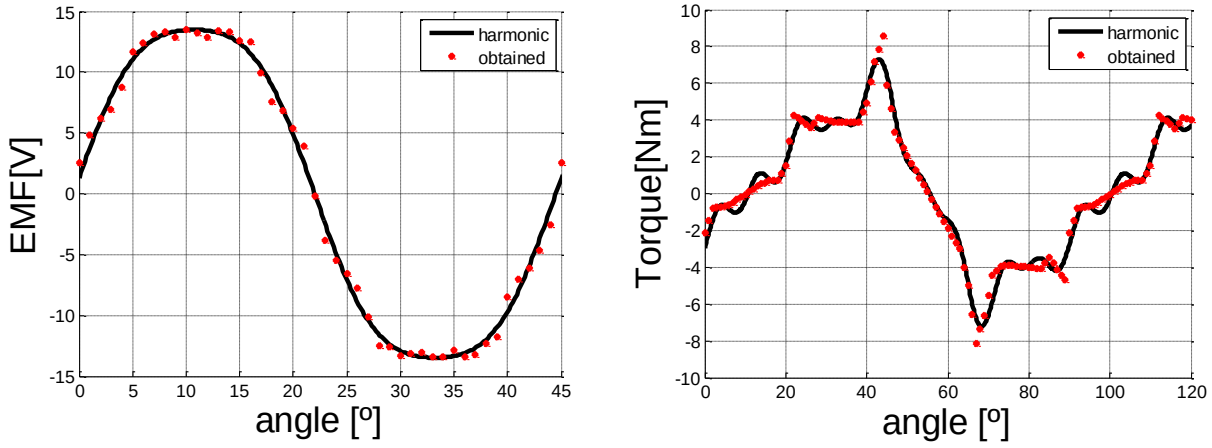

(a) (b)

Figure 37- Conversion of the signal recovered from the 3D FEM study to its most significant harmonic components of the 4 legs model: (a) EMF, (b) Torque

In the 4 leg machine model, one could connect all windings in series. However the same does not apply to the 6 legs one. The new 6 legs model will require either 3 or 6 phases, due to the distribution of the legs around the rotor. On the other hand, while on the 4 legs model the effect each leg has on the torque ripple adds to the next, the newer model's stator leg distribution will further reduce the existing torque ripple. This will be further explained and showed in the next two sections.

3.2.1 EMF

In the 4 legs model, the distribution of the stator legs, allied with the 8 salience rotor configuration synchronizes the output EMF of each leg. Therefore, it would be convenient to connect them all in series, the resulting EMF will resemble the one in Figure 37 (a) but now multiplied by 4 as seen in Figure 38 (a). The same does not apply to the 6 legs one, as shown in Figure 38 (b).

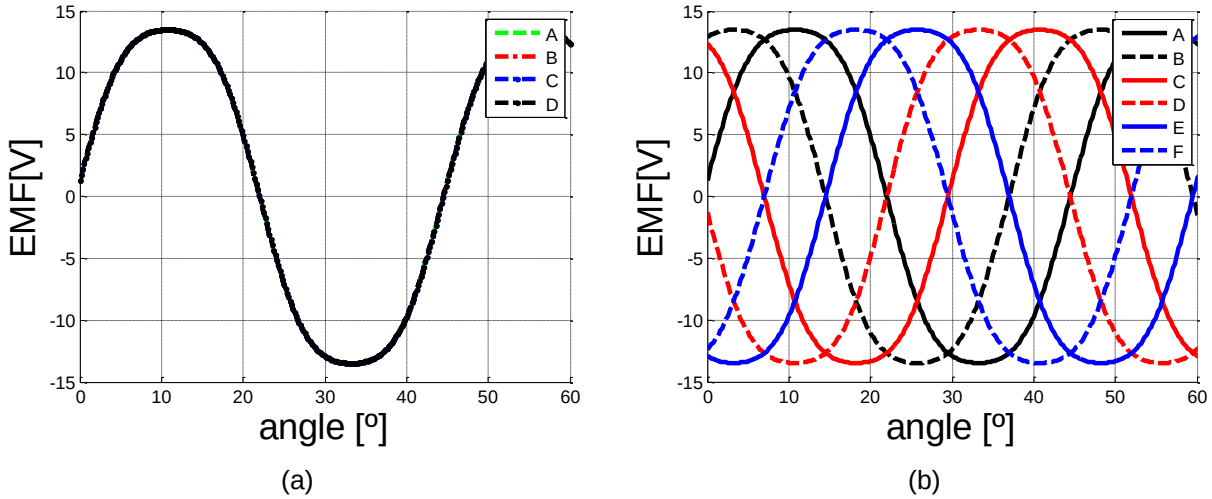

Figure 38- EMF of each independent leg, for: (a) 4 legs model; (b) 6 legs model.

Adding the EMF of all legs in the 4 legs model will result in the one seen in Figure 39 (a). On the other hand, adding an extra pair of legs creates, as seen in Figure 37 (b), a discrepancy of 60º in each leg's EMF phase. Connecting them in series would result in them cancelling each other out. The alternative will be to either have each leg treated separately, treating it as a 6 phase system or, combining them in triples, to create two 3 phase system, as seen in Figure 39 (b).

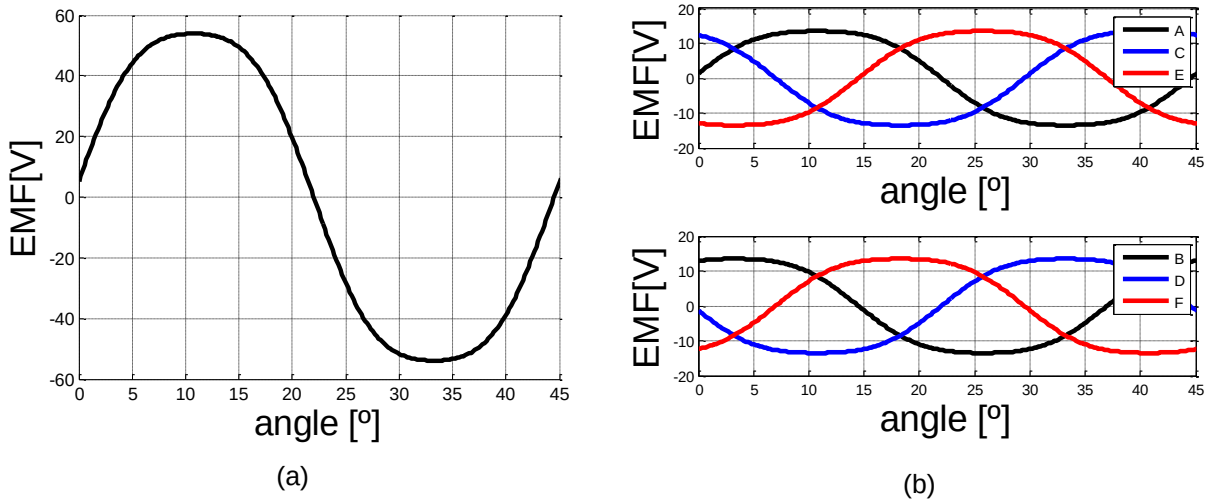

Figure 39- Resulting EMF in each machine model, when no electric load is applied at 3000rpm: (a) 4 legs model (single phase); (b) 6 legs model (2 three phases systems).

3.2.2 Torque ripple

Unlike the EMF, the two model's resulting torque ripple have different periods. Due to the way the stator's legs of both machine models are distributed, the influence each is going to have on a rotor salience is different, as seen in Figure 40. The 4 legs stator exhibits a higher amplitude, this occurs because the legs are further apart, decreasing the magnetic energy in a salience while it's between legs. On the other hand the 6 legs stator, has a smaller amplitude, because its legs are closer together.

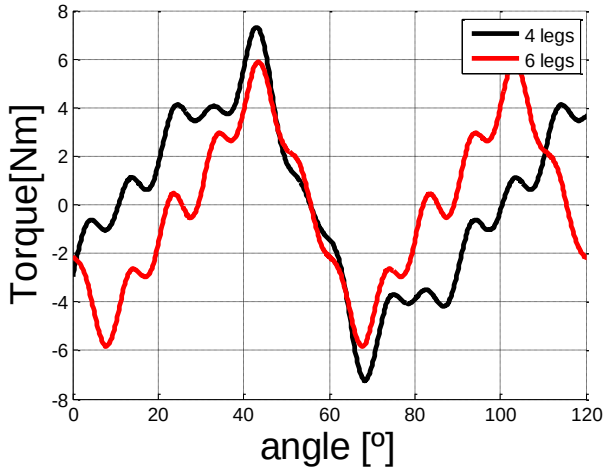

Figure 40- Torque evolution in one of the rotor's salience for the 4 legs model and the 6 legs model.

With the 4 legs stator, in Figure 41 (a), rotor saliences can be divided into two groups of 4: 1,4,5,8 and 2, 3, 6, 7. In the 6 legs stator's case the saliences can be grouped in four pairs: 1, 5; 2, 6; 3, 7 and 4, 8. For Figure 41 only the top rotor will be shown with the legends corresponding to the rotor numbered in Figure 35.

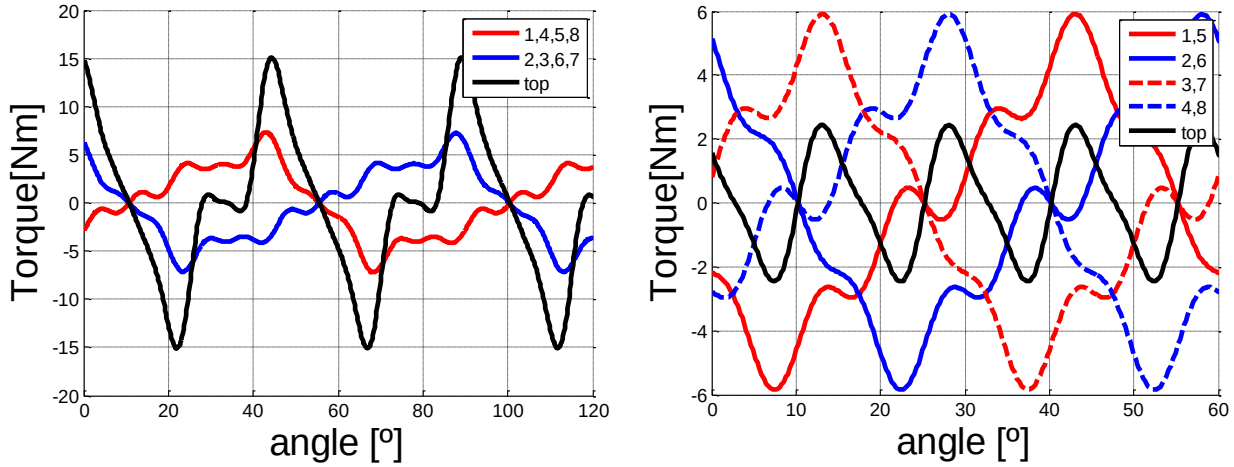

(a) (b)

Figure 41 – Torque ripple effects in the top part of the rotor, each salience individually their combined contribution: (a) 4 legs stator, (b) 6 legs stator.

Even though individually, the behaviour of the torque ripple on each rotor saliences for the different models, is fairly similar. However when combining them, the same does not occur. Figure 41 (a) and (b) show that while in the 4 legs machine the total top oscillation value increases, in the 6 legs machine the torque ripple decreases. This effect is due to leg placement, the strongest harmonic of each salience, instead of combining into a stronger one, just like what happens to the 4 legs model, cancel each other out.

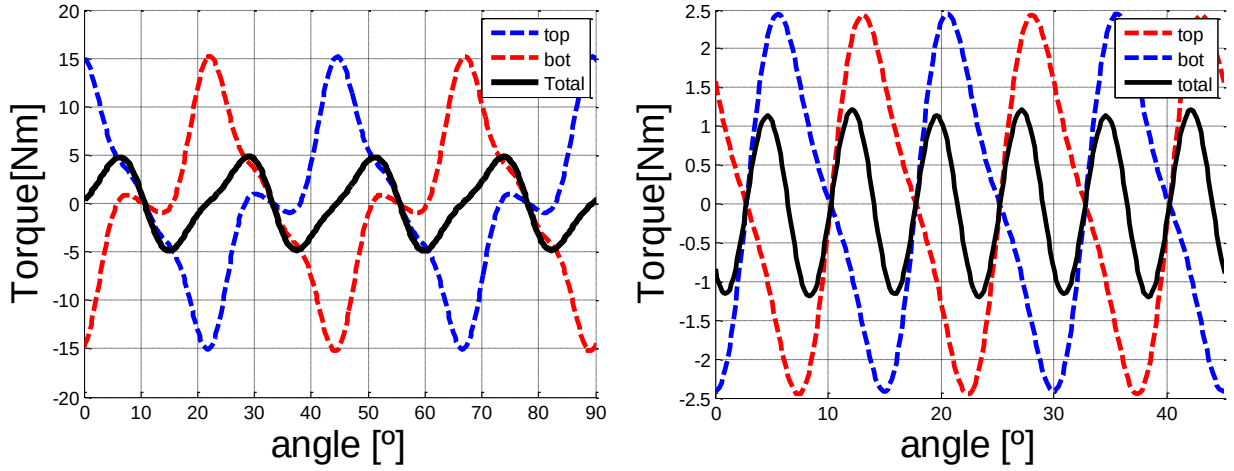

(a) (b)

Figure 42- Torque behaviour with no electrical load at 3000rpm for the two machine models: (a) 4 legs; (b) 6 legs.

By combining the top and bottom halves, the expected value for the total torque ripple of each machine model is obtained and shown in Figure 42. In both cases the torque ripple value greatly decreases. When comparing the two machines, it is clear, the 6 legs one is a better choice when trying to reduce torque ripple.

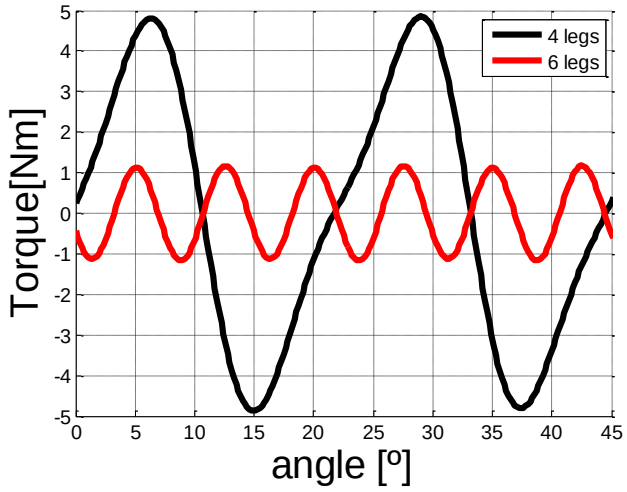

Figure 43- difference in the resulting torque ripple when no load is applied on each model.

On the other hand, the frequency of both increase since the most significant harmonics are atoned. Table 8 demonstrates the how, even though the torque ripple has a higher variation rate, its RMS plummets.

Table 8-comparission of the RMS of the two models.

Legs	**EMF/turn RMS** (V)	**Torque ripple RMS (Nm)**			**Materials** ($\mathbf{dm^3}$)			
		Individual rotor salience	Individual rotor	Total	Iron		Copper	NdFeB
					Laminated(rotors)	Soft(stator)		
4	41.904 (1 phase)	3.74	7.81	3.16	12.759	16.177	8.984	0.112
6	10.476 (6 phase)	3.17	1.72	0.87 (-72.78%)	12.759	24.266 (+50%)	13.476 (+50%)	0.168 (+50%)

To sum up, by adding a pair of legs to the stator, the performance of the model is expected to greatly increase. Not only is expected a 50% increase in the power output per winding turn, it is also expected a significant decrease in the torque ripple affecting the model. All this without significantly increasing the materials used.

4 Effect of an electric load on the generator's operation

The EMF waveform for the different legs share the same harmonics content, but differ in phase. As a result, directly connecting all windings would not be beneficial, since the sum of every wave would erase the EMF. Therefore, it was adopted two three phase electrical connection for the windings. Maximizing the EMF per phase is crucial. Hence, by observing the waves in Figure 38 (b), the chosen connections would be as marked in Figure 44 (a) and (b). Since six legs are available they will be divided into two three-phase (3Ø) independent systems. Each coil them can be identified with a code: 3Ø system [1, 2]; phase [a, b, c]; leg [A, B, C, D, E, F]; there is also an arrow, under the rubric of Ampere's right hand to determine the turning direction of the coil's winding. Coils sharing the same stator leg are series connected.

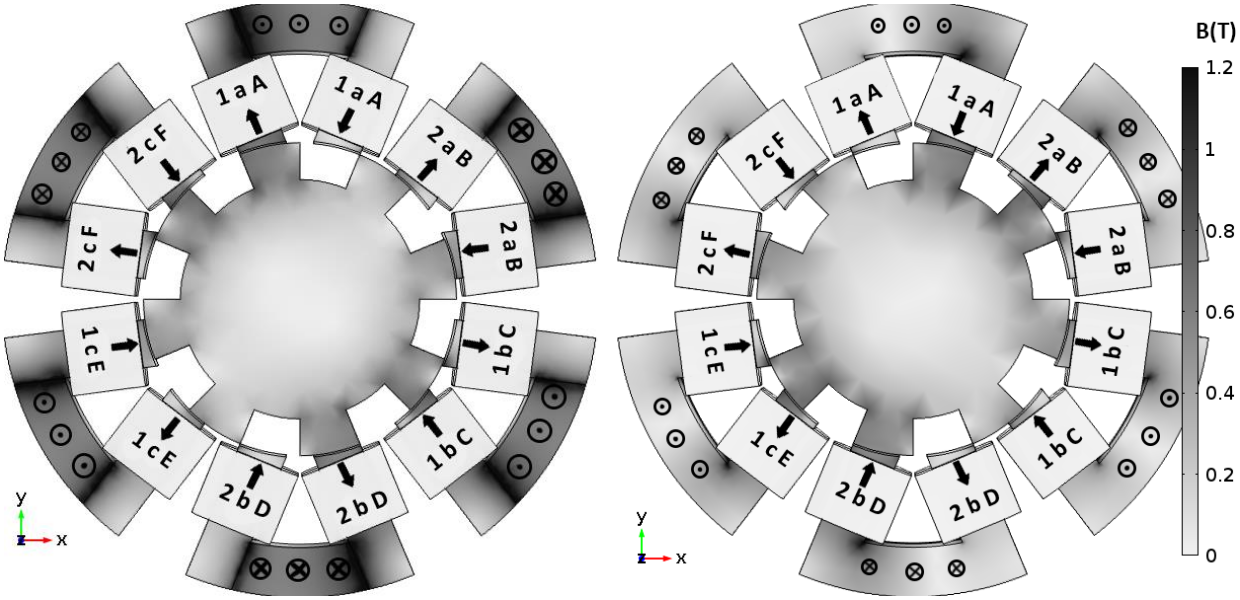

(a) (b)

Figure 44- Windings configuration and phase configuration for the 6 legs generator: (a) bottom part; (b) top part.

In order to obtain the most out of each stator leg, the coils have to be arranged properly. Since the legs share a topology the EMF relation between the stator poles of each leg is replicated to the others. Therefore, the configuration found for a stator leg can be mimicked. Figure 45 shows the EMF for each pole of a stator leg, considering one clockwise rotation turn per coil.

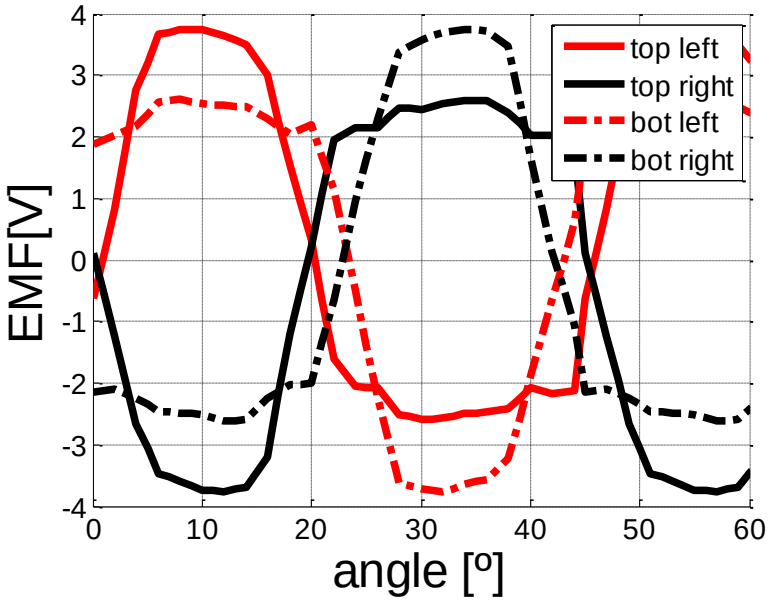

Figure 45 – EMF of each stator leg's pole

By analysing Figure 45, it can be assumed the best series connection possible is, by inverting the rotation of both right coils, of each stator, to counter-clockwise, as shown in Figure 46. Since all legs are similar the connections within each leg is the same and considering the left side of the coil as the positive electric pole and the right as the negative, the series connection is exemplified in Figure 46.

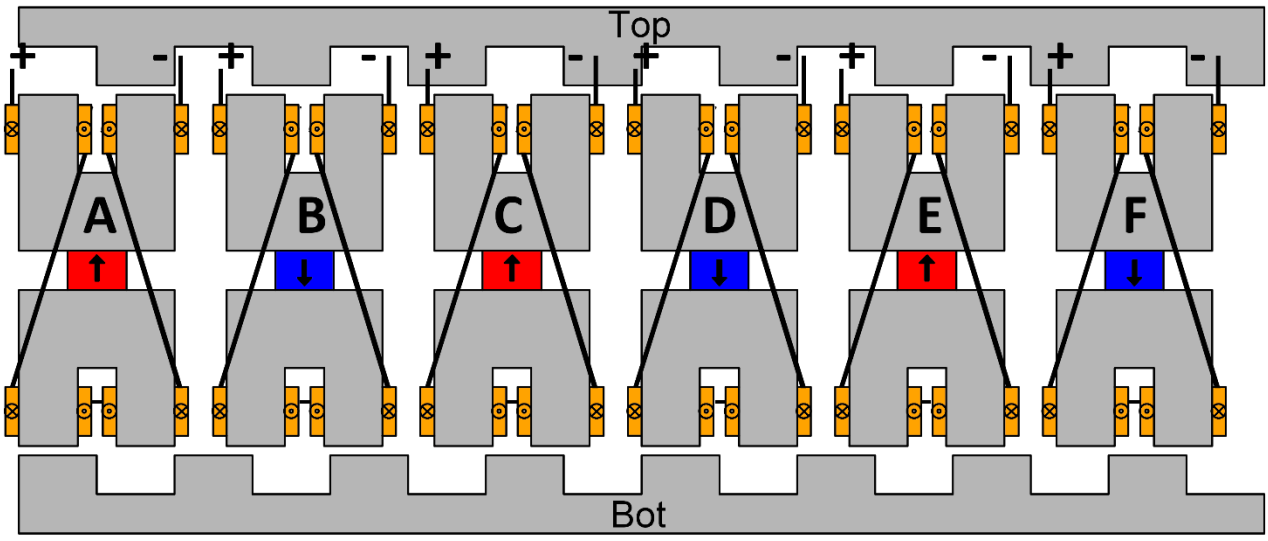

Figure 46- Illustrative linear representation of the electrical connections between windings each leg.

The resulting EMF induced at each leg is again showed in Figure 47. When comparing the different EMF signals, their amplitude is equal but with different phases. Each leg as a 60º discrepancy between one another.

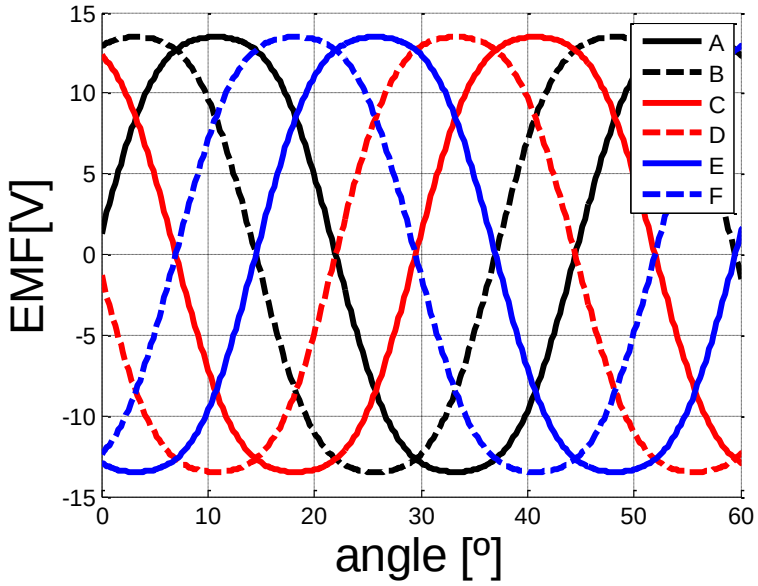

Figure 47- Wave form of the EMF for each stator's leg.

Examining the phase waveforms, the stator legs can be assembled into two groups of three: [A, C, E] and [B, D, F]. Using the first 3Ø system as an example, the connections would be as followed: A's positive pole connected to phase 'a' of the first 3Ø system; C's positive pole connected to phase 'b' of the first 3Ø system; E's positive pole connected to phase 'c' of the first 3Ø system; the negative poles from this three legs will all be star connected. Table 9 - Connections to form the two three phase summarizes the establish connection in order to create the two 3Ø system with 120º phase difference between each phase. Figure 46 shows the required connection in order to maximize the EMF output per leg.

Table 9 - Connections to form the two three phase systems.

Leg	Three phase system	Phase
A	1	A
B	2	A
C	1	B
D	2	B
E	1	C
F	2	C

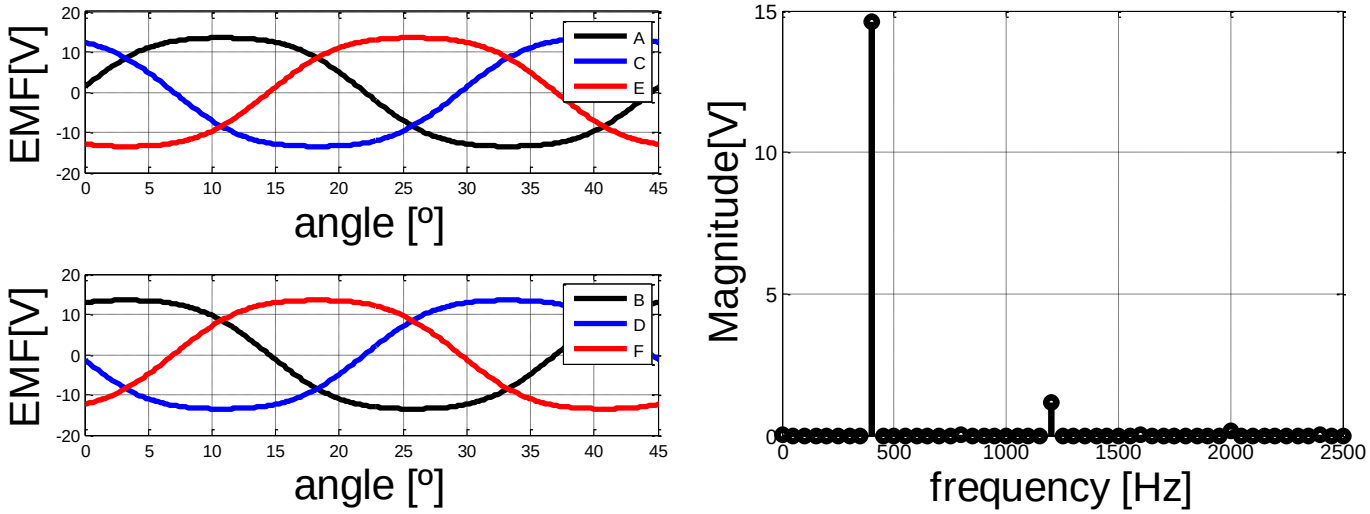

(a) (b)

Figure 48- (a) EMF of each phase of the machine when no electrical load is attached; (b) FFT of a phase of the generator's EMF, with no electrical load

Figure 48 (a) displays the two 3Ø systems of the simulated model. The waveforms are practically sinusoidal, as the FFT spectrum of the wave supports, shown in Figure 48 (b). However, instead of the typical 120º phase difference between each wave, they show a 60º phase difference. Figure 48 (b) shows there are two most significant wave harmonics: 400 Hz and 1200 Hz.

4.1 Electrical system used to study the 6 phase generator while connected to a load.

The FEM software was coupled with an electric circuit block simulation tool that allows for a better understanding of the effect in the generator operation under an unbalanced electric load. Even though applying an electrical load in the finite element program was not possible for a 3D study, an electric current density could be imposed in each winding to simulate the effect of an electric load connected to the generator. However, to compute these currents using the electric circuit block simulation tool, an equivalent electric model of the synchronous generator design must be used and subdued to a power converter system and its electric load. The main use of this type of generators is at high speeds, the solid rotor is capable of withstanding high centrifugal forces and one of the industries that would benefit from a better understanding of this generators is the aeronautics'. Therefore, the electric load used is a simplified version of the electric components of a commercial airplane Boeing 767, also used before in [7]. This load is not balanced, hence, the power converter will provide a uniform distribution of the electric current amongst the different windings of the generator. The rotation speed of the generator will be fixed at 3000 rpm, which will result in an electric frequency signal of 400 Hz.

4.1.1 The power converter system

For the generator, it was considered the equivalent thevenin's circuit of a synchronous machine, composed of six independent phases, with one ac voltage sources in series, representing the first harmonic, and a RL branch to symbolize the windings influence on the EMF.

The chosen rectifier is a 12 pulse rectifying bridge found in [8]. This rectifier provides a smother DC level, and due to the transformers, one can increase the voltage output of the machine, decreasing current in windings, consequently joule losses. The DC level shown in Figure 49 is composed by a capacitor, followed by a DC/AC inverter. With this connection even with an unbalanced load, the current in the machine stays evenly distributed. After the oscillator a low pass filter is crucial in order to remove the high frequency harmonics.

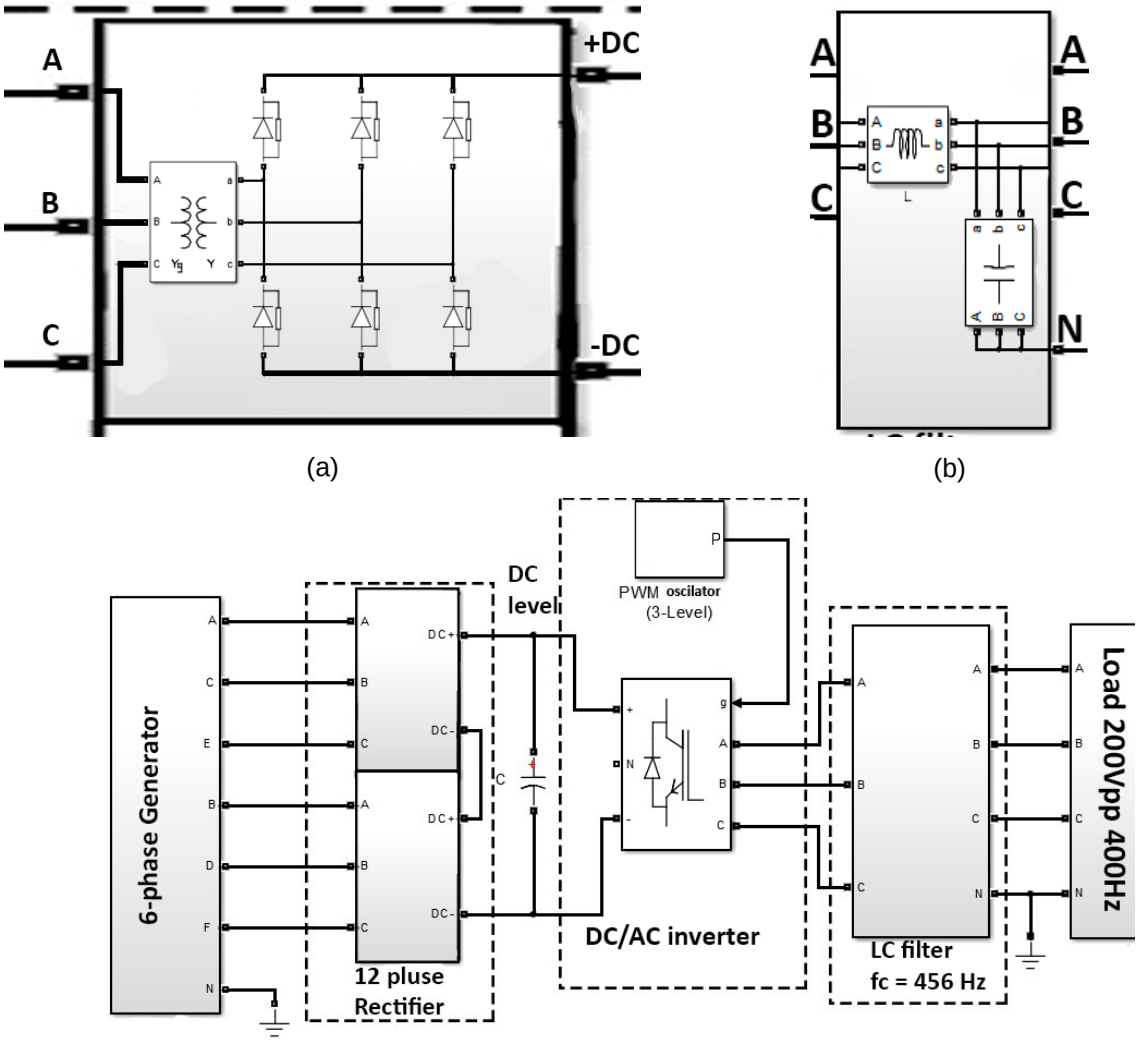

Figure 49- AC/AC converter proposed for each phase of the generator, with the output of 115 V, 400Hz: (a) part of the 12 pulse rectifier; (b) LC filter; (c) complete AC/AC converter.

For the proper usage of the power converter, the calculation of the filters is mandatory. The DC level will help keep a constant voltage at the entry of the inverter and the LC filter will remove the high frequency components injected in the load. The low pass filter was obtain using a L-C Filter Calculator, available at [9], where the cut off frequency was aimed to be around 456 Hz in order to let the 400 Hz wave pass.

As for the calculation of the capacitor on the DC level, it is important to keep the voltage input of the inverter levelled. Through simulation it was reached the value of 600 mF that kept the voltage decay under 5%. The obtain values for the other electrical components are explicit in Table 10- Sizing of the filter components in the AC/AC converter. Being 'm' the transformation relation between the generator and the converter and the 'L' and 'C' of the filter, the reach values required to obtain the cut off frequency 456 Hz.

Table 10- Sizing of the filter components in the AC/AC converter

m	C	L(filter)	C(filter)
0.1	600 mF	15 μH	9 mF

4.1.2 The electrical load

The full use of the 6 phase generator designed will be at high velocities. Hence, in order to simulate its behaviour and establish it viability, just like in dissertation [7], it will be used the same electrical load and turbine engine characteristics of a Boeing 767 as described in [10]. Its electrical load can, as seen in Figure 50- Simplified electric equivalent load of a Boing 767 plane, be divided into: three 3ø RL loads, one 1ø RL load and one 12 pulse converter connected to a couple of R loads, as specified in Table 11.

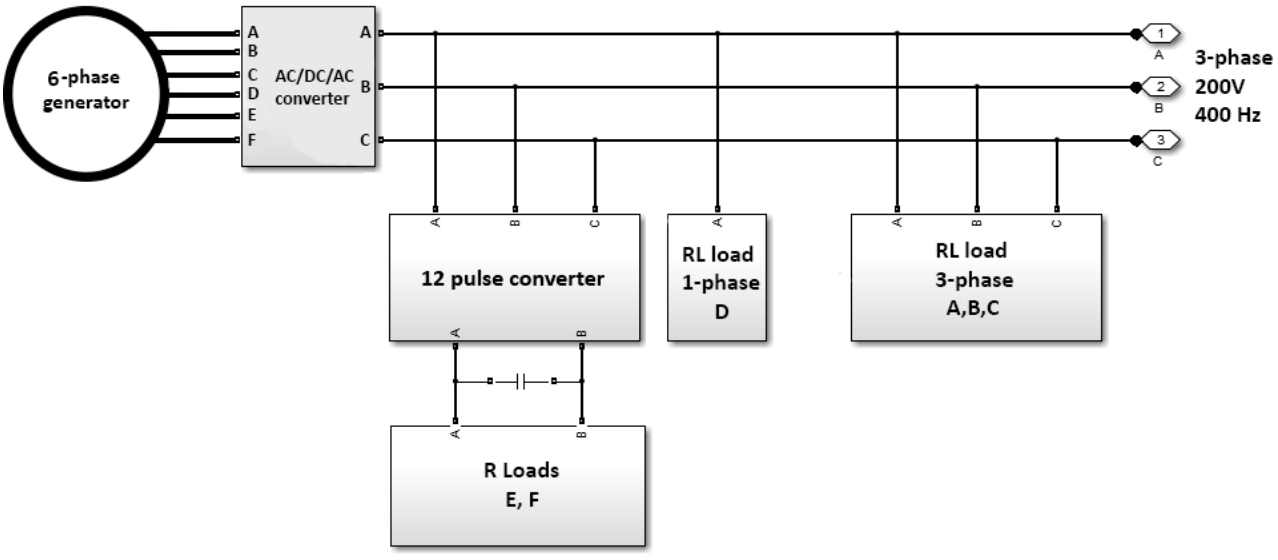

Figure 50- Simplified electric equivalent load of a Boing 767 plane.

Table 11- Load values for the simplified model of a Boeing 767 in [10], for a power supply of 90kVA.

Load	Phase	R(Ω)	L(mH)
A	A	0.84	0.304
	B	2.41	1.065
	C	2.49	1.129
B	A	14.28	2.752
	B	14.28	2.752
	C	14.28	2.752
C	A	2.15	0.597
	B	1.91	0.712
	C	1.91	0.712
D	A	4.34	0.504
	B	-	-
	C	-	-
E	-	0.068	-
F	-	0.076	-

The AC/AC converter from Figure 49, applied to the generator, provides a reasonable prediction of the injected currents. By feeding said currents to the FEM analysis it is possible to study the effect they would have on the magnetic flux and torque. The EMF is directly related to the magnetic flux, therefore understanding the effect these currents will have on the generator is fundamental.

4.2 FEM study of the electrically loaded 3D 6 legs generator

Once electric currents are taken into consideration, due to the generator's electric load, its presence will change the magnetic flux distribution throughout the machine. This new magnetic flux distribution can not only provoke a demagnetization of the PM but also drastically increase power losses in them. Furthermore, the flux created by the electric currents will influence the behaviour of the magnetic field in the soft iron core, which could consequently affect the efficiency of the generator as a result of magnetic saturation or EMF reduction.

The reduction of EMF is due to the back-EMF. The back-EMF is the result of the magnetic flux variation created by the current in the windings. This normally opposes to the one generated by the PM and movement of the rotor. As is evident in Figure 51 (a) and (b) the flux generated by the currents opposes the one from the PM. By only considering the influence of the current in the windings, it is safe to assume the magnetic flux mainly closes its path on a pair or stator poles while the from the PM needs to connect to go through another stator leg. With that in mind and observing Figure 51 (a) and (b) it is clear, on the left arm the fluxes contradict each other but on the right they are concordant. This means the magnetic flux variation will decrease due to current in the windings thus reducing the EMF.

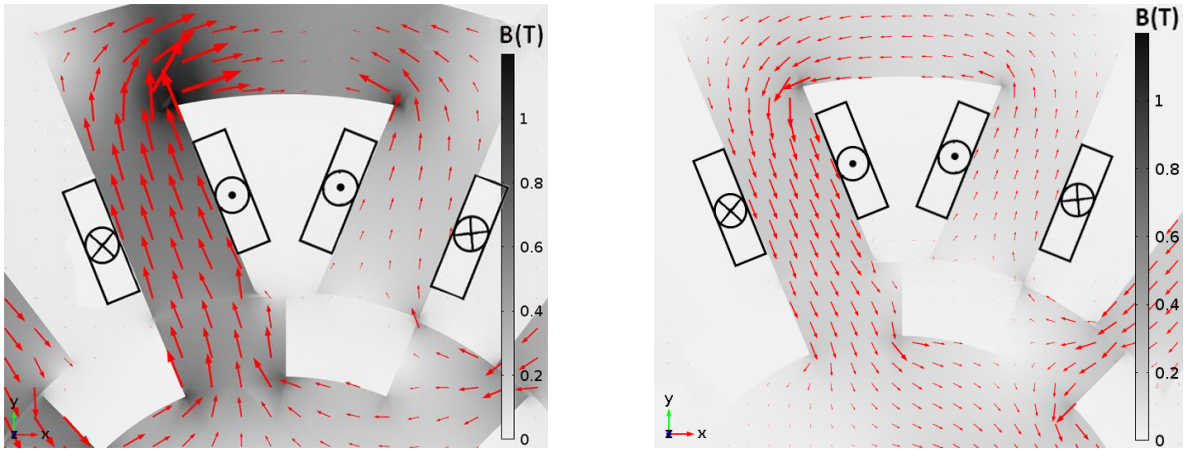

(a) (b)

Figure 51- Magnetic flux stream, red arrows, for the different contributors: (a) Permanent Magnets; (b) current in windings.

Since windings' flux opposes the ones generated by the PM it can be assumed the back-EMF contradicts the EMF. Therefore the resulting magnetic field will, be weaker than the one without currents reducing the level of saturation. Considering without a load the magnetic field intensity did not exceed the knee of the BH curve, with load, this value should not be transposed.

4.2.1 Effect of currents in the armature winding on the EMF

As seen in Figure 49 the injected currents in each 3ø system is different although seemly different their RMS is almost equal being (a) and (b) respectively 24.03 A and 24.02 A. The biggest relevance is the phase difference they will impose in the magnetic flux.

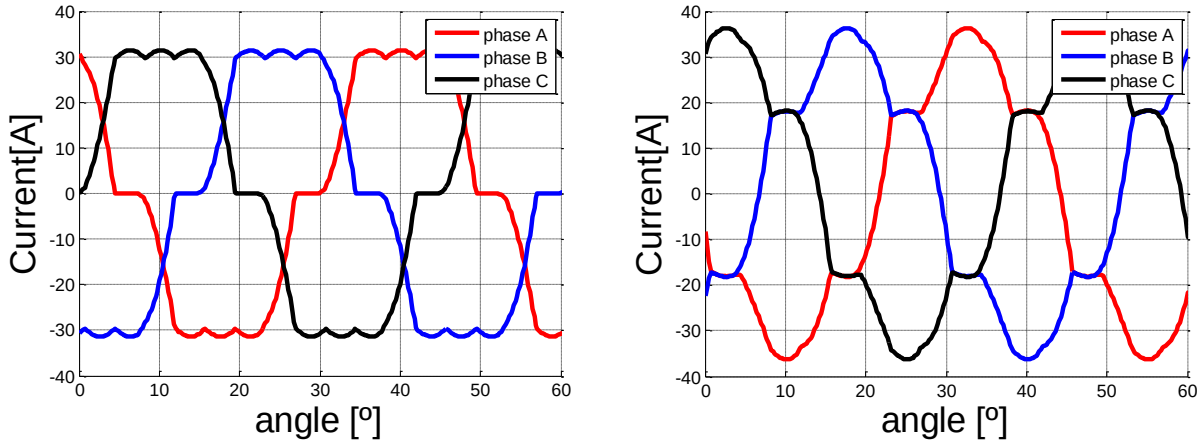

(a) (b)

Figure 52 – Injected current in the generator due to the application of the electric load at 3000 rpm: (a) first 3ø system, rms 24.03 A; (b) second 3ø system, rms 24.02 A.

The perfect harmonic exhibit in the no load case, got significantly changed, due to the effects of the currents. Not only did the main harmonic get reduced but a third was added, furthermore the phase of the wave was shifted around 10º to accommodate the current effect.

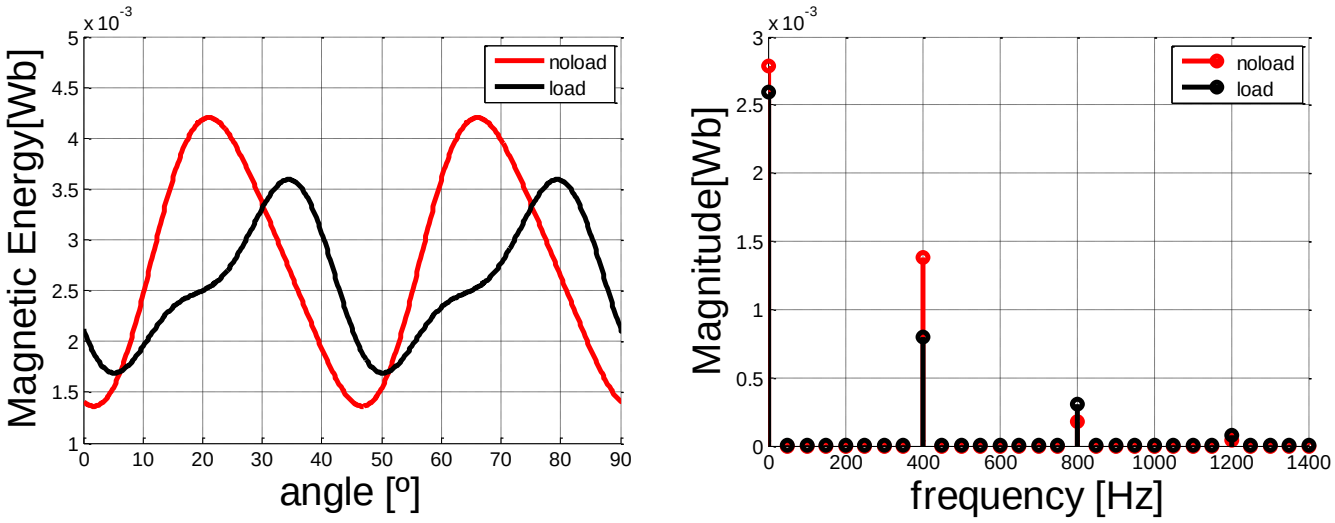

Figure 53 – Magnetic flux variation in one of the stator legs arms: (a) signal, (b) FFT sample

The influence of the magnetic flux created by the current circulating in the winding changed the magnetic flux circulation resulting in a significant change in the EMF. The current in the winding generated back-EMF reducing the 1º harmonic and increasing the 3º. The difference between the two is evident in Figure 54 (a) and (b) and Table 12.

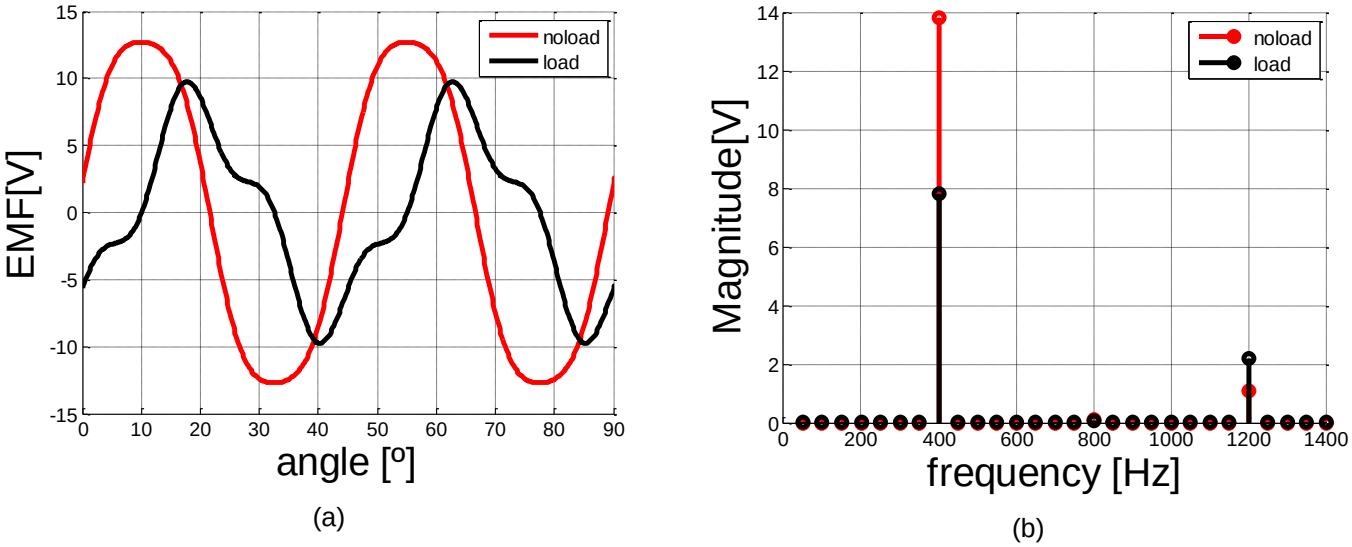

Figure 54 – EMF per turn reaction due to the effect of the coils with and without an electric load, at 3000 rpm: (a) waveform; (b) FFT signal.

Table 12 - EMF reaction due to the effect of the coils with and without the presence of the electric load.

	No load	With load
$\mathbf{EMF_{ef1^{o}h}}$ [V]	9.13	5.51 (−40%)
$\mathbf{EMF_{ef3^{o}h}}$ [V]	0.48	1.55 (+223%)
$\mathbf{EMF_{ef}}$ [V]	9.14	5.73(−37.3%)

In order to reduce the current level in the windings without considerably affecting the power output or power losses, increasing the insulation temperatures, it was considered a high number of turns per coil. Since the EMF decreased, due to applying the electric load, in order to maintain the current levels, the number of turns was double. Using a Simulink model simulation of the electrical characteristics of the values reached were as stated in table 13 and Figure 49.

Table 13 – New electrical characteristics of the model due to application of a load.

Turn per coil	EMF RMS (V)	Current RMS (A)	Apparent power (kVA)
80	731.2	24.02	105.38

4.2.2 Effect of currents in the armature winding on the torque ripple

The presence of currents in the windings change the magnetic flux distribution in the generator. The effect this new distribution will have on the torque ripple of a single rotor piece can be seen in Figure 55 (a) and (b). The main thing that stands out is the increased value in torque ripple associated with the electric load.

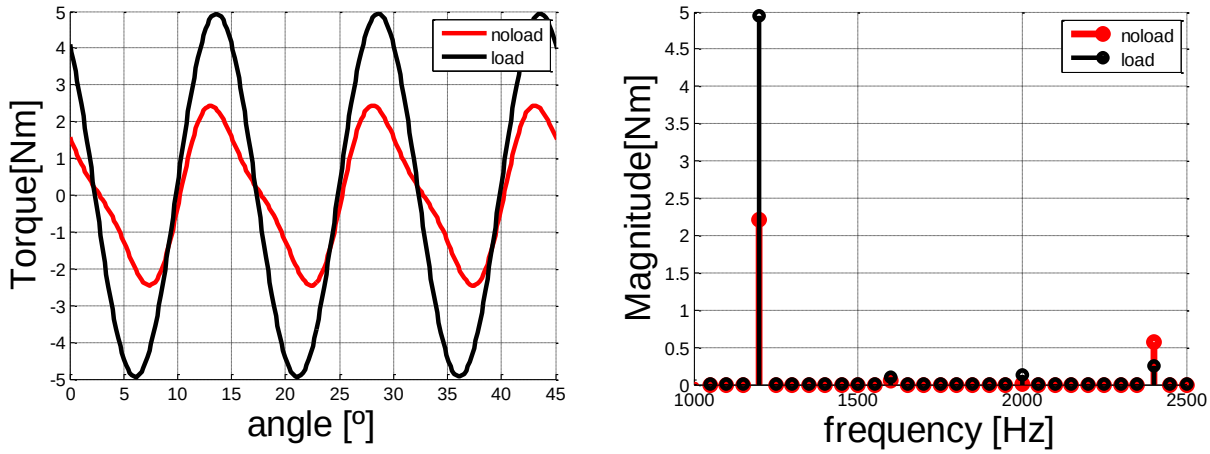

Figure 55- Torque ripple in the top rotor of the generator: (a) waveform, (b) FFT signal.

The current alters the behaviour of the magnetic energy of the model. The presence of current in the windings increases the main harmonic component, and filters the other ones. To better understand this, it is easier to divide the rotor into its 8 saliences. The difference in the magnetic energy dispersion in each salience between having a load or not is expressed in Figure 56.

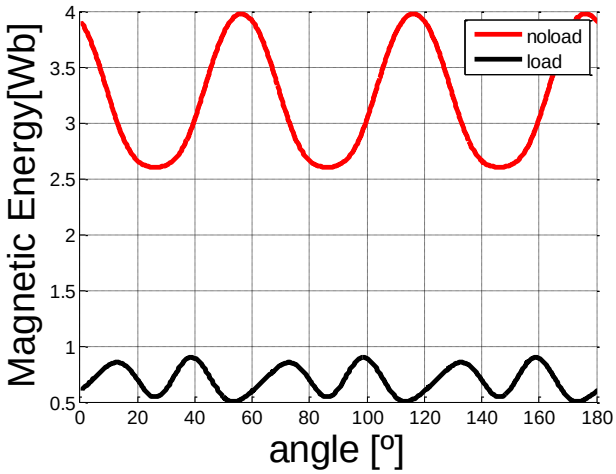

Figure 56-Magnetic Energy density in a salience, difference between having or not an electrical load attached to the model.

Since the torque ripple is obtain from the magnetic energy it is easy to assume, even though the variation rate in the no load case is higher, its wave form is fairly more regular than when a load is applied. This will result in, as seen in Figure 57, a much strong harmonic component in the load case.

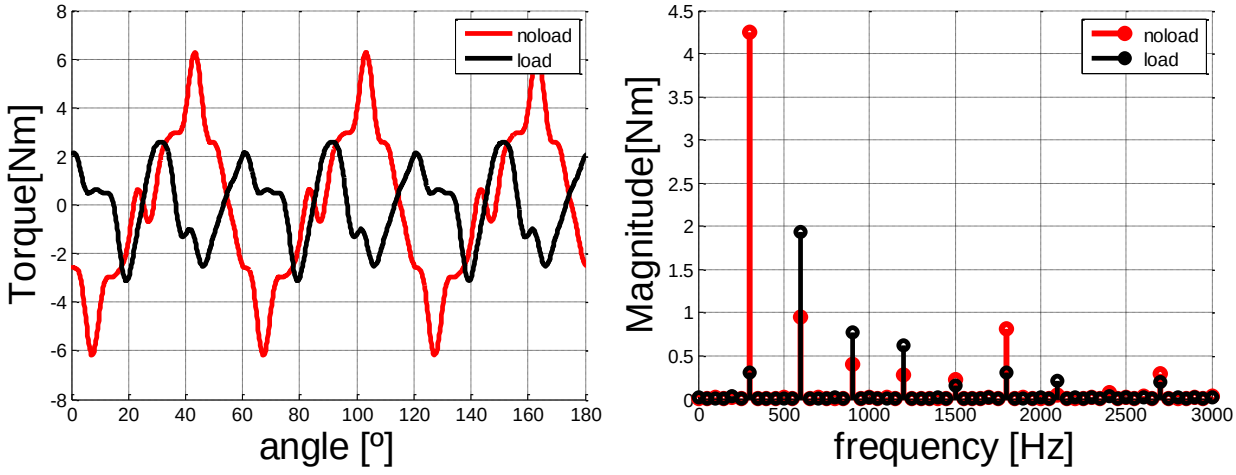

(a) (b)

Figure 57- Torque ripple for a salience in the rotor: (a) waveform, (b) FFT signal.

Considering each salience has a 60º phase discrepancy, by combining all saliences, the resulting torque is the one in Figure 49. In both cases the only two harmonics that don't get counteracted are the 4th and 8th, respectively at 1200 Hz and 2400 Hz. Combining the results from the top rotor with the bottom rotor, it is obtained the expected value for the expected total torque ripple of the model.

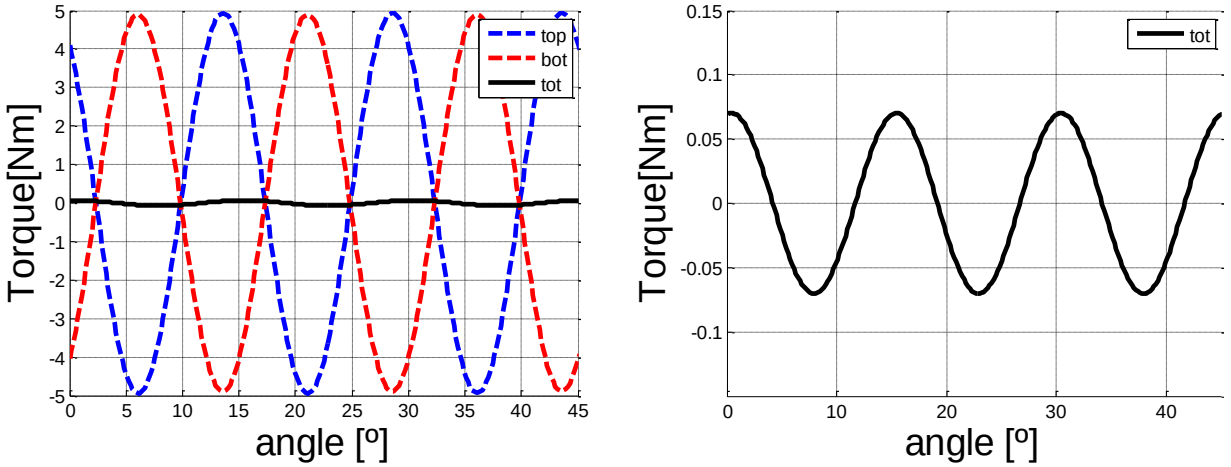

(a) (b)

Figure 58-Resulting torque ripple for: (a) both rotors; (b) the complete model.

Since individually, both rotors have the torque ripple waveform practically sinusoidal and are 180º apart. Adding the two significantly decreases the effect of the other, considering each wave represents torque ripple of a rotor, the total torque ripple felt by the model can be considered insignificant.

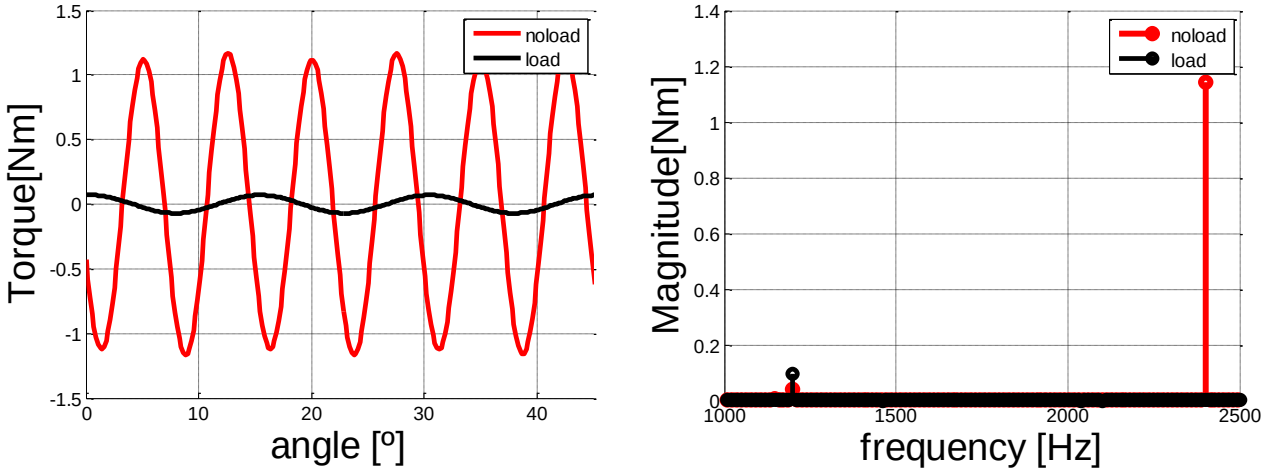

(a) (b)

Figure 59- Torque ripple for a salience in the rotor: (a) waveform, (b) FFT signal.

4.2.3 Temperature/ Power loss

Due to having a higher level of EMF, the current in the winding is fairly low, as a result, even though the resistance of the windings is bigger, the Power losses in the windings would be considerably small. However both, permanent magnets and the soft-iron, are susceptible to losses due to induced currents in the iron fragments.

In order to obtain the thermal behaviour of the operating model one would have to obtain, not only the power losses but also the heat dissipation capacity. Using a natural convection heat transfer coefficient estimation calculator, downloaded from [12], it is possible to compute the natural convection heat transfer. The obtained value is seen in table 14. As for the power losses, those have to be divided into several categories: windings, rotor saliences, stator saliences, magnets and stator body.

The winding losses are given by the joule heating formula while the others are from the manufactures power loss per kg per magnetic field variation in [13] and are presented in table 14 as well. The losses in the soft-iron, 3P Somaloy, are 46 W/T/kg, the permanent magnets will be assumed to have the same characteristics as the soft-iron. What was noted while evaluating the magnetic flux variation in Figure 53 – Magnetic flux variation in one of the stator legs arms: (a) signal, (b) FFT sample divided by the cross-section of the saliences was 0.25 T.

Table 14 – Parameters for the thermal analysis of the generator with a 90kVA electric load, with natural convection heat transfer.

$\mathbf{h(W/(m^2 * K))}$	Windings (W)	Rotor saliences (W)	Stator saliences (W)	Stator body (W)	Magnets(W)
5.77	399.2	585.1	677.4	658.8	115.6

The components with the loads thermal limit are the windings insulation which are a little over 100ºC. With that said, the aim should be to keep the temperature under 100ºC. This is not possible with a natural convection heat transfer, since a thermal simulation situates the overall temperature over 239ºC. Having in mind the specification for the load, mentioned in chapter 4.1, the machine, when operating, will have a constant flow of cold air passing through it, this will increase the convection heat transfer, serving as the cooling system required by the machine.

The convection heat transfer coefficient needed, in order to, have enough dissipation is between 13 and $15\ W/(m^2K)$. For a low speed flow of air over a surface the value of convection heat transfer is $10\ W/(m^2K)$ and for moderate speed $100\ W/(m^2K)$, as referenced in [14]. Since the generator is directly coupled to the turbine, it can be assumed the air flow, it will be subdued to, is strong, placing the convective heat transfer coefficient over $100\ W/(m^2K)$.

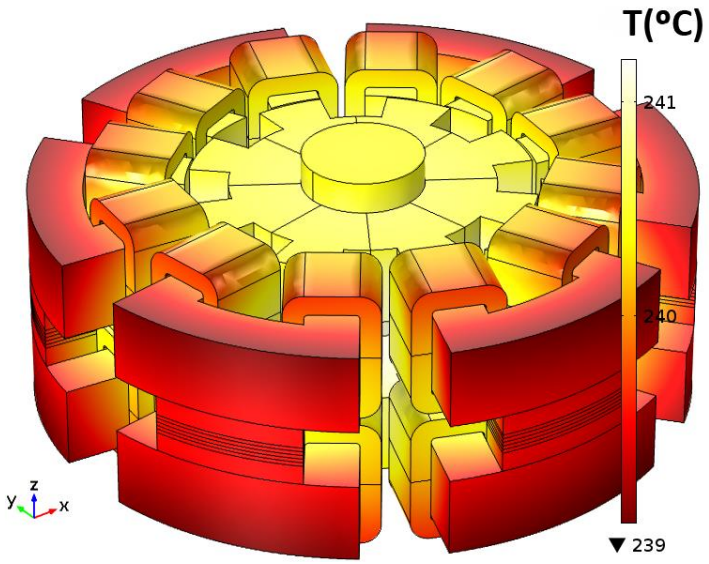

Figure 60- Heat distribution in case convection heat transfer is natural ($5.77\ \mathrm{W/m^2K}$)

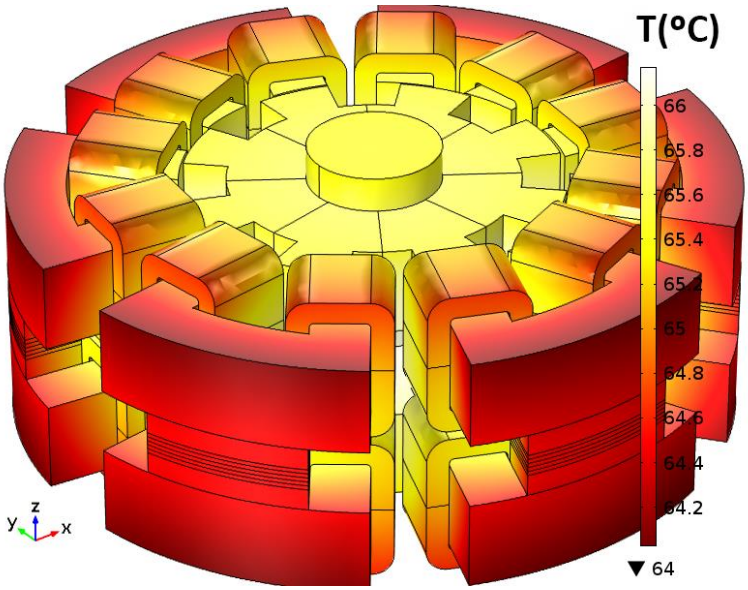

Figure 61 -Heat distribution for forced convection heat transfer ($15\ \mathrm{W/m^2K}$)

Preforming the FEM thermal analysis of the generator, it is clear without forced cooling it would be impossible to keep the generator active. However with a small cooling system the generator can be kept on without the fear of damaging the cable insulation or demagnetizing the permanent magnets.

5 Conclusions

5.1 Final analysis of the study

Electric machines with permanent magnets and concentrated windings in the stator are commonly known for their high torque ripple. However the model reached shows significant improvements in that regard specially while carrying and electric load. While normally the effects of the load increases the torque ripple, with the design presented the torque ripple is insignificant when compared with the nominal torque provided by the planes turbine.

Reducing the magnetic energy variation limited the production of EMF, which resulted in an increased number of turn per coil to reduce the injected current. This current, simulates the application of the load and reduced the EMF RMS by 37% reviling a high contribution of the back-EMF, created by the currents in the windings.

The initial thermal analysis supports the idea of a need to have force cooling the system. However, since the machine is design to integrate a turbine axis, the model will have a stream of cold air passing through its gaps, potentially abolishing the need for additional cooling systems.

Overall the model reached its main objective, but the size of the model could turn out to be problematic. There are some improvements required for it to be considered a viable machine, nevertheless the results support the possibility for this design to be a plausible solution for the torque ripple problem in Permanent Magnets flux switching Generated.

5.2 Future work

As mentioned before the size of the model and its high dependence on the injected currents are easily the issues that need to be addressed. To do so only one aspect needs to be improved, the variation of magnetic flux. The main focus should be them:

- Optimising the length of the magnets;
- Change the rotors configuration;
- Increase the number of legs in the stator.

By increasing the length of the magnets, one can increase their contribution on the magnetic flux flow, however in doing so, one must take into consideration the magnetic saturation and the path chosen by the magnetic flux.

Changing the rotor configuration can increase the magnetic flux variation, however the major setback is the increased torque ripple. The proposed rotor would be as seen in Figure 62 (b), opposed to the minimal torque ripple solution reached in Figure 62 (a). One would have to outweigh their differences to see if the change is valid.

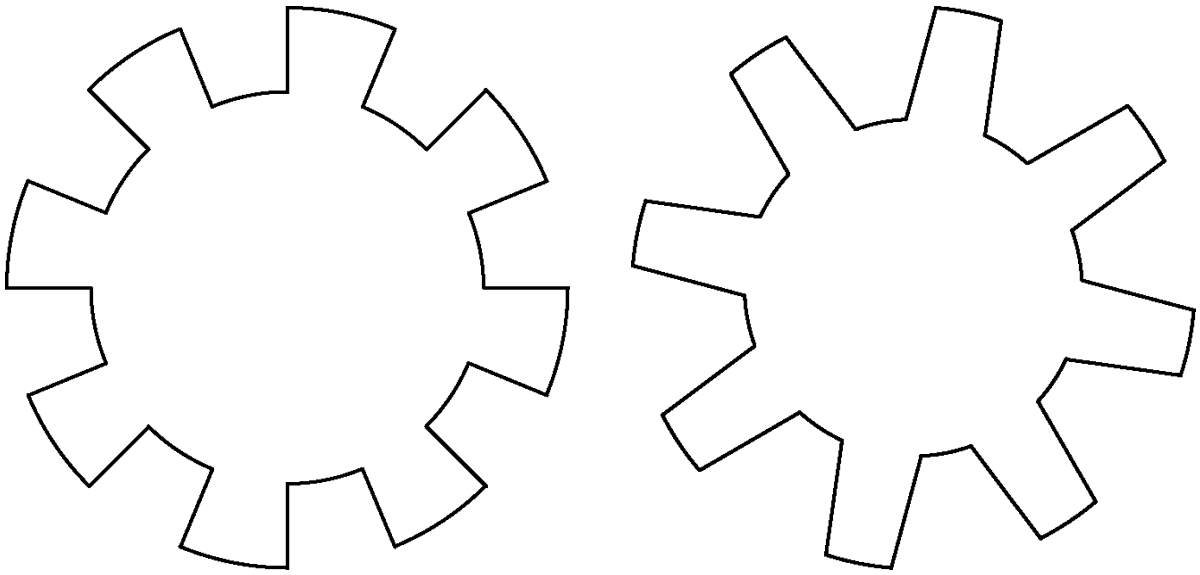

(a) (b)

Figure 62- Rotor configuration for different machines behaviours: (a) minimal torque ripple; (b) maximum EMF.

The studied model was developed to minimize torque ripple, therefore, in its complexity, the design was always taught with a minimalistic perspective. Based on the study made and the results obtained, it is expected that by keeping the number of legs as multiples of 6 the torque ripple should stay at the same level as it is right now.

References

[1] S. E. Rauch, L. J. Johnson “Design Principles of Flux-Switch Alternators” Published in: Transactions of the American Institute of Electrical Engineers. Part III: Power Apparatus and Systems (Volume: 74, Issue: 3) Date of Publication: Jan. 1955 IEEE

[2] Ricardo Jorge Nunes Maurício “O gerador Elétrico de Reluctância com Magnetos Permanentes”, MSC Dissertation in Electrical and computing Engineering, Institute Superior Tecnico, University of Lisbon, October 2012

[3] Jing Zhao, Yashuang Yan, Bin Li “Influence of Different Rotor Teeth Shapes on the Performance of Flux Switching Permanent Magnets Machines Used for Electric Vehicles” School of Automation, Beijing Institute of Technology, Beijing, Published: 1 December 2014, www.mdpi.com/journal/energies

[4] W. Fei, P.C.K. Luk “Permanent Magnet Flux Switching Integrated-Starter-Generator with Different Rotor Configurations for Cogging Torque and Torque Ripple Mitigations” Published: Energy Conversion Congress and Exposition, 2010 IEEE

[5] H. Jia, M. Cheng, W. Hua, W. Zhao and W. Li “Torque Ripple Suppression in Flux-Switching PM Motor by Harmonic Current Injection Based on Voltage Space-Vector Modulation”, IEEE Transactions on Magnetics(Volume 46, Issue: 6), June 2010

[6] N. Larsen, A. Gensior, P Hein “Torque ripple reduction based on current control for a flux switching permanent magnet machine” Power Electronics, Electrical Drives, Automation and Motion, June 2012 International

[7] Luís Carlos Silva Pinto “Integrated Electrical Generators in Aircraft Turbines” ”, MSC Dissertation Electrical and computing Engineering, Institute Superior Tecnico, University of Lisbon, October 2015

[8] José Pedro Sucena Paiva “Redes de Energia Eléctrica: uma análise sistémica”, Second edition, ISTPress, December 2007

[9] (2016, Apr.). L-C filter calculator [Online]. Available: http://circuitcalculator.com/lcfilter.htm

[10] A. Eid, M. Abdel-Salam, H. El-Kishky, T. El-Mohandes “Simulation and transient analysis of conventional and advanced aircraft electric power systems with harmonic mitigation” Electric Power Systems Research, Volume 79, Issue 4, April 2009, Pag: 660-668

[11] (2016, Apr.). PowerStream, ‘American Wire Gauge’ 2015. [Online]. Available: http://www.powerstream.com/Wire_Size.htm

[12] (2016, Apr.). Bright Hub Engineering [Online]. Available: http://www.brighthubengineering.com/hvac/92660-natural-convection-heat-transfer-coefficient-estimation-calculations

[13] (2015, Jul.). Somaloy® Technology [Online], Hoganas AB (Sweden). Available:https://www.hoganas.com/en/business-areas/soft-magnetic-composites/

[14] (2016, Apr.). Engineers EDGE [Online], Convective Heat transfer Coefficients Table Chart. Available: http://www.engineersedge.com/heat_transfer/convective_heat_transfer_coefficients__13378.htm